Article

Cell Chemical Biology

Stabilization of the Max Homodimer with a Small Molecule Attenuates Myc-Driven Transcription

Graphical Abstract

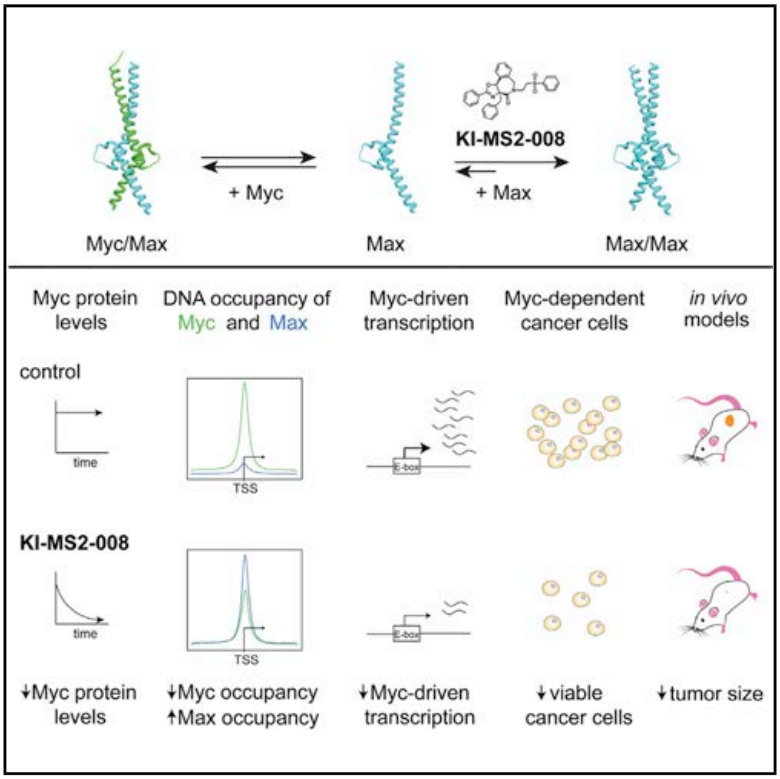

Highlights

- KI-MS2-008 is a Max-binding small molecule that attenuates Myc-driven transcription
- The compound stabilizes the Max homodimer
- Effects on DNA occupancy and the transcriptome resemble loss of Myc
- Treatment with KI-MS2-008 exhibits efficacy in cellular and murine cancer models

Authors

Nicholas B. Struntz, Andrew Chen, Anja Deutzmann, ..., Charles Y. Lin, Dean W. Felsher, Angela N. Koehler

Correspondence

koehler@mit.edu

In Brief

Myc/Max-mediated transcription is deregulated in most of human cancers. Struntz et al. discovered a small molecule that stabilizes the Max homodimer and attenuates Myc-driven transcription with efficacy in cellular and murine cancer models. This discovery reinforces an alternative Myc-targeting strategy and could inform development of compounds to treat Myc-dependent cancers.

Struntz et al., 2019, Cell Chemical Biology *26*, 1–13
May 16, 2019
https://doi.org/10.1016/j.chembiol.2019.02.009

CellPress

Please cite this article in press as: Struntz et al., Stabilization of the Max Homodimer with a Small Molecule Attenuates Myc-Driven Transcription, Cell Chemical Biology (2019), https://doi.org/10.1016/j.chembiol.2019.02.009

Cell Chemical Biology
Article

Stabilization of the Max Homodimer with a Small Molecule Attenuates Myc-Driven Transcription

Nicholas B. Struntz,[1,2,3,13] Andrew Chen,[1,2,3,13] Anja Deutzmann,[4] Robert M. Wilson,[1,2,3] Eric Stefan,[1,2] Helen L. Evans,[1,2,3] Maricela A. Ramirez,[5] Tong Liang,[5] Francisco Caballero,[1,2] Mattheus H.E. Wildschut,[1,2] Dylan V. Neel,[1,2] David B. Freeman,[1,2,6] Marius S. Pop,[1,2,6] Marie McConkey,[7,8,9] Sandrine Muller,[9] Brice H. Curtin,[1,2,3] Hanna Tseng,[1,2] Kristen R. Frombach,[1,2] Vincent L. Butty,[1,10] Stuart S. Levine,[1,10] Clementine Feau,[9] Sarah Elmiligy,[1] Jiyoung A. Hong,[1,2,11] Timothy A. Lewis,[9] Amedeo Vetere,[9] Paul A. Clemons,[9] Scott E. Malstrom,[1] Benjamin L. Ebert,[7,8,9] Charles Y. Lin,[5,12] Dean W. Felsher,[4] and Angela N. Koehler[1,2,3,9,14,*]

[1]David H. Koch Institute for Integrative Cancer Research, Massachusetts Institute of Technology, Cambridge, MA 02142, USA
[2]Department of Biological Engineering, Massachusetts Institute of Technology, Cambridge, MA 02139, USA
[3]MIT Center for Precision Cancer Medicine, Massachusetts Institute of Technology, Cambridge, MA 02142, USA
[4]Division of Oncology, Departments of Medicine and Pathology Stanford School of Medicine, Stanford, CA 94305, USA
[5]Department of Molecular and Human Genetics and Verna & Marrs McLean Department of Biochemistry and Molecular Biology, Baylor College of Medicine, Houston, TX 77030, USA
[6]Kronos Bio, Inc., Cambridge, MA 02139, USA
[7]Division of Hematology, Department of Medicine, Brigham and Women's Hospital, Harvard Medical School, Boston, MA 02115, USA
[8]Department of Medical Oncology, Dana-Farber Cancer Institute, Boston, MA 02215, USA
[9]Broad Institute of MIT and Harvard, Cambridge, MA 02142, USA
[10]BioMicro Center, Massachusetts Institute of Technology, Cambridge, MA 02142, USA
[11]Division of Pediatric Hematology/Oncology, Boston Children's Hospital, Boston, MA 02115, USA
[12]Therapeutic Innovation Center, Baylor College of Medicine, Houston, TX 77030, USA
[13]These authors contributed equally
[14]Lead Contact
*Correspondence: koehler@mit.edu
https://doi.org/10.1016/j.chembiol.2019.02.009

SUMMARY

The transcription factor Max is a basic-helix-loop-helix leucine zipper (bHLHLZ) protein that forms homodimers or interacts with other bHLHLZ proteins, including Myc and Mxd proteins. Among this dynamic network of interactions, the Myc/Max heterodimer has crucial roles in regulating normal cellular processes, but its transcriptional activity is deregulated in a majority of human cancers. Despite this significance, the arsenal of high-quality chemical probes to interrogate these proteins remains limited. We used small molecule microarrays to identify compounds that bind Max in a mechanistically unbiased manner. We discovered the asymmetric polycyclic lactam, KI-MS2-008, which stabilizes the Max homodimer while reducing Myc protein and Myc-regulated transcript levels. KI-MS2-008 also decreases viable cancer cell growth in a Myc-dependent manner and suppresses tumor growth *in vivo*. This approach demonstrates the feasibility of modulating Max with small molecules and supports altering Max dimerization as an alternative approach to targeting Myc.

INTRODUCTION

Max is a transcription factor that acts as a critical hub in a bHLHLZ transcription factor network capable of binding different interaction partners in response to stimuli (Conacci-Sorrell et al., 2014). Most notably among these is Myc, a master regulator of growth and proliferation. Myc binds DNA as an obligate heterodimer with Max, and this heterodimer recognizes canonical E-box sequences (CACGTG) (Blackwell et al., 1990) abundant throughout the genome and enriched at promoters of growth and proliferation genes. Although Max preferentially heterodimerizes with Myc, Max can also form homodimers that effectively block Myc/Max heterodimers from binding to DNA, thus attenuating transcriptional activity (Figure 1A) (Cascón and Robledo, 2012). In addition, Max can form heterodimers with the Mxd family of proteins (Nair and Burley, 2003), which recruit additional transcriptional repressors to actively shut down transcription (Laherty et al., 1997). Deregulation of Myc/Max-mediated transcription can lead to tumorigenesis through activation of cardinal hallmark features of cancer including cellular growth, proliferation, self-renewal, and evasion of apoptosis (Dang, 2012; Gabay et al., 2014). As such, a longstanding goal of the cancer research community has been to directly target Myc. Inactivation of Myc in model systems with engineered gene regulation (Felsher and Bishop, 1999) or expression of the dominant negative peptide Omomyc appears to elicit oncogene addiction and tumor regression (Soucek et al., 2002), and,

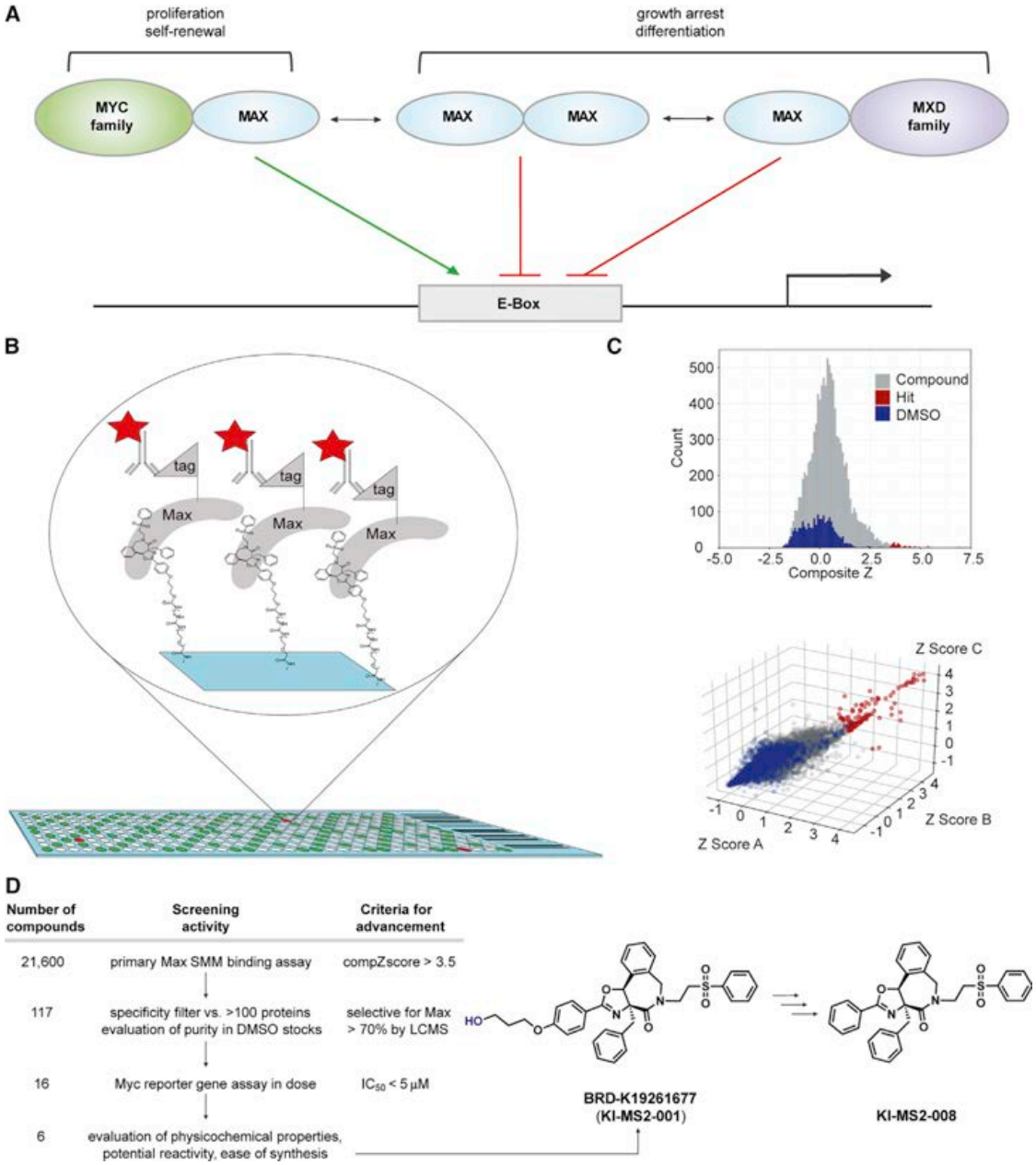

Figure 1. Discovery of a Putative Max Binder

(A) Cartoon diagram of the Max (blue) dimerization network displaying transcriptional activation by the Myc (green)/Max heterodimer, transcriptional attenuation by the Max/Max homodimer, and transcriptional repression by Max/Mxd (purple) heterodimer.

(B) Schematic of a small molecule microarray (SMM) showing SMM positives (red spots), which were detected by Alexa Fluor 647-labeled antibodies against the His-tag on the purified Max protein.

(C) SMM screening results for DIV06 compound library, which is comprised mostly of products of diversity-oriented synthesis (n = 3 technical replicates). Histogram of composite *Z* scores and 3D scatterplot showing *Z* scores of feature to background ratios in triplicate for compounds on the SMMs.

(D) Prioritization scheme for Max binders that modulate Myc-driven transcription leading to hit stock solution **BRD-K19261677** (resynthesized as **KI-MS2-001**) and **KI-MS2-008** as a more potent and synthetically accessible probe.

See also Figures S1–S4 and Table S1.

in fact, Myc is one of the few oncogenes for which true oncogene addiction has been demonstrated *in vivo* (Felsher, 2010; Soucek et al., 2008). Myc is highly regulated and degrades rapidly (Farrell and Sears, 2014), so a dynamic equilibrium shift away from Myc/Max transcriptional activation can occur by inhibiting the Myc/Max interaction directly or by inducing either Max/Max homodimers or Max/Mxd heterodimers (Conacci-Sorrell et al., 2014). The vast majority of small molecule inhibitors developed to inhibit Myc transcriptional activity have focused on disrupting the Myc/Max interaction (ex. 10058-F4, 10074G5, KJ-Pyr-9,

and sAJM589) (Choi et al., 2017; Hart et al., 2014; Yin et al., 2003), but strategies to stabilize other Max dimers—such as stabilization of the Max/Max homodimer with NSC13728 (Jiang et al., 2009)—remain relatively unexplored. Utilizing a chemical probe to directly target Max will clarify its role in this dynamic equilibrium and improve our understanding of the transcriptional consequences of perturbing various Max protein interactions.

While modulating Myc/Max-mediated transcription via a Max-directed small molecule is an appealing alternative approach to targeting Myc directly, these transcription factors have proven difficult to target due to their intrinsically disordered nature that lack traditional binding pockets and systematic design strategies to perturb protein-protein or protein-DNA interactions (Darnell, 2002; Koehler, 2010; McKeown and Bradner, 2014). In recent years, the small-molecule microarray (SMM) platform has helped bridge this gap by enabling robust and unbiased binding assays capable of identifying small molecules with multiple modes of binding regardless of how disordered or intractable a target may be, thus making it an attractive screening approach compared with other traditional binding assays such as differential scanning fluorimetry (Hong et al., 2014). This high-throughput approach utilizes glass slides functionalized with small molecules to permit fluorescent detection of protein-small molecule interactions (Figure 1B) (Vegas et al., 2008). This screening approach has been previously used to identify small molecule binders to proteins, DNA, and RNA, including binders to the ETV1 transcription factor, Hedgehog growth factors, and G-quadruplexes, among others (Felsenstein et al., 2016; Pop et al., 2014; Stanton et al., 2009).

RESULTS

Discovery of Max Binders that Modulate Myc-Driven Transcription

We used SMMs to screen purified recombinant Max protein against 21,600 printed chemical array features, including commercial compounds, known bioactives, natural products, products of diversity-oriented synthesis (DOS) (Clemons et al., 2010), and various negative controls, which yielded 117 putative Max binders (Figures 1C and S1A). After prioritizing assay positives specific to Max as compared with more than 100 other proteins screened against the same set of molecules, we identified six compounds that inhibited Myc transcriptional activity with a half maximal inhibitory concentration (IC_{50}) less than 5 μM in a dual luciferase reporter assay containing tandem Myc response elements (Figures S1B–S1D). We prioritized the DOS polycyclic lactam **BRD-K19261677** (**KI-MS2-001**) (Mitchell and Shaw, 2006) due to validated potency on resynthesis and reasonable physicochemical characteristics (Figures 1D and S1E).

To establish cursory structure-activity relationships (SARs), we synthesized analogs of **KI-MS2-001** (Figure S2). Using the same Myc transcriptional dual luciferase reporter assay as an indicator of compound activity, we identified sites tolerant to modification and determined that the propanediol side chain, which is predicted to mediate attachment to the SMM surface, was not required for activity (Figure S3; Table S1). Removal of this group allowed **KI-MS2-008** to be synthesized by a simplified pathway (8 versus 13 steps), which improved overall yield from 4% to 51%, while slightly improving the reporter IC_{50} value to 1.28 μM (Figures 2A and 2E). The enantiomers of **KI-MS2-001** and **KI-MS2-008** demonstrated comparable activity with the racemic mixture when tested separately (Figure S3; Table S1). As seen by the CellTiter-Glo assay to measure ATP as an indicator for metabolically active cell levels (Riss et al., 2013), both compounds decreased levels of viable P493-6 cells, a well-characterized B cell line engineered with exogenous c-Myc under a doxycycline-repressible promoter (Schuhmacher et al., 1999), with **KI-MS2-008** displaying an IC_{50} value of 2.15 μM after 3 days of treatment (Figures 2B and 2E). The effect of **KI-MS2-008** was lost with co-treatment of doxycycline, which shuts down expression of c-Myc (Figure 2D), as well as in EBNA2-driven cells that proliferate without exogenous c-Myc with co-treatment of both doxycycline and β-estradiol (Pajic et al., 2000) (Figure S4A), suggesting that c-Myc inhibition is the primary mechanism underlying diminished growth of viable cells. In contrast to levels of viable cells, P493-6 cell viability—as measured by propidium iodide exclusion—was unaffected by compound treatment (Figure S4B). The PC12 rat pheochromocytoma cell line (Hopewell and Ziff, 1995), which lacks functional Max protein (Figure 2D), was insensitive to treatment with both compounds (Figures 2C and 2E), suggesting the possibility of on-target effects in cells. In addition, we evaluated the viable cell levels of a variety of other cancer cell lines upon treatment with both compounds (Figures S1F, S1G, S4C, and S4D) in CellTiter-Glo assays. As a preliminary assessment of specificity, we profiled **KI-MS2-008** (10 μM) for activity against a panel of 299 kinases followed by dose-response experiments for selected kinases. **KI-MS2-008** did not inhibit any of these kinases with an IC_{50} value below 10 μM (Figures S4E and S4F). These initial findings encouraged us to further characterize **KI-MS2-008** as a Max-directed small molecule that modulates Myc transcriptional activity.

KI-MS2-008 and Analogs Engage Max *In Vitro* and in Live Cells

Although the parent compound was discovered in a target-directed primary screen, we used five approaches to validate the hypothesis that **KI-MS2-008** directly engages Max. The first two strategies made use of previous SAR studies to develop chemical probes for both affinity-enrichment experiments in cell lysates and photo-crosslinking studies in live cells (Figures S2 and S3; Table S1). We conjugated **KI-MS2-081**, an analog containing a primary amine (Figure 3A), to NHS-activated magnetic beads and incubated **KI-MS2-081**-loaded and unloaded control beads with P493-6 cell lysates to pull down protein targets of the compound. We observed Max, as well as c-Myc, bound to **KI-MS2-008**-loaded beads as determined by immunoblots (Figure 3B). Pull down of Max with these compound-loaded beads was similarly observed when doxycycline was used to repress c-Myc expression. We also synthesized **KI-MS2-085**, a bifunctional probe containing a diazirine for UV-activated covalent attachment to neighboring proteins (Mackinnon and Taunton, 2009), and an alkyne handle for copper-catalyzed azide-alkyne cycloaddition to a fluorophore for visualization (Figure 3C). To determine the validity of this approach, purified full-length Max was covalently linked to **KI-MS2-085** and

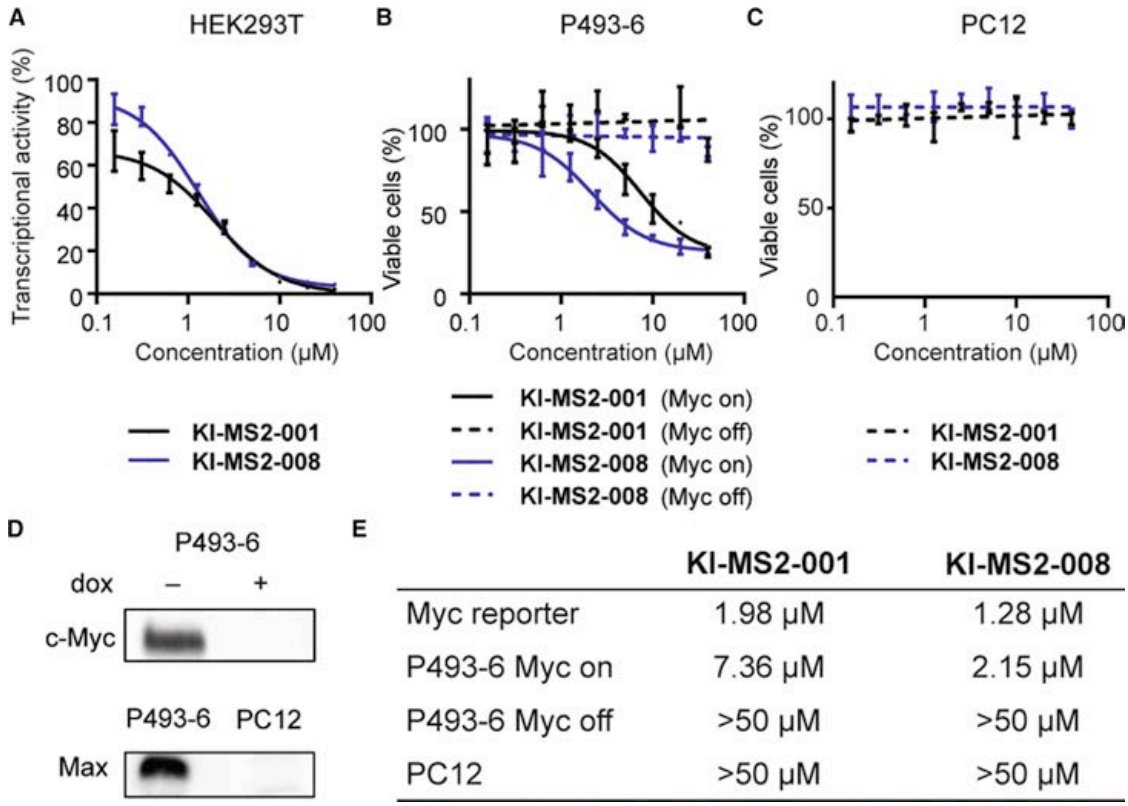

E

	KI-MS2-001	KI-MS2-008
Myc reporter	1.98 μM	1.28 μM
P493-6 Myc on	7.36 μM	2.15 μM
P493-6 Myc off	>50 μM	>50 μM
PC12	>50 μM	>50 μM

Figure 2. KI-MS2-001 and KI-MS2-008 Modulate Myc-Driven Transcription in Cells and Inhibit Viable Cell Levels in a Myc-Dependent Manner

(A) Dose-response curves for the Myc dual luciferase reporter assay in HEK293 cells in response to **KI-MS2-001** or **KI-MS2-008** treatment after 16 h (n = 3 technical replicates, error bars represent mean ± SD).

(B) Dose-response curves for P493-6 viable cell levels in response to **KI-MS2-001** or **KI-MS2-008** treatment with Myc expression left on or shut down with doxycycline after 3 days (n = 3 technical replicates, error bars represent mean ± SD).

(C) Dose-response curves for PC12 viable cell levels in response to **KI-MS2-001** or **KI-MS2-008** treatment after 5 days (n = 3 technical replicates, error bars represent mean ± SD).

(D) Immunoblots of c-Myc from P493-6 lysates, demonstrating doxycycline repressed expression of c-Myc and immunoblots of Max from P493-6 and PC12 lysates, showing the lack of functional Max in PC12 cells.

(E) Summary of estimated IC_{50} values for the Myc reporter assay and viable cell levels.

See also Figure S4.

conjugated to Alexa Fluor 647, which was visualized by SDS-PAGE. Mass spectrometry was used to confirm the presence of a covalent protein-small molecule adduct (Figures S5A and S5B). After validation of covalent reaction with pure protein, P493-6 cells were treated with **KI-MS2-085** (2.5, 5, and 10 μM) followed by irradiation for covalent linkage in cells. Following cell lysis, the same workflow allowed visualization of a pair of proteins between 20 and 25 kDa (Figure 3D). These proteins matched the molecular weights of two Max isoforms and aligned with immunoblot-based detection of these Max isoforms (Figure S5C). The intensities of these bands varied in a dose-dependent manner, were not observed without UV irradiation, and were reduced by co-treatment with competitive **KI-MS2-008** (40 μM) (Figure 3D).

In addition, we used a cellular thermal shift assay (Molina et al., 2013) to determine whether **KI-MS2-008** produced ligand-induced thermal stabilization of Max in P493-6 cells. We demonstrated that **KI-MS2-008** stabilized cellular Max in a dose-responsive manner, further suggesting engagement to Max (Figures 3E and S5D). Looking at the effects of stabilizing Max in a time-dependent manner, we observed that the stabilization of Max occurs at about 30 min after initial dosing of **KI-MS2-008**, possibly leading to a subsequent destabilization of c-Myc starting at 45 min (Figures 3E and 5A).

In preliminary efforts to identify a possible binding site of **KI-MS2-008** on Max, we used NMR spectroscopy and mass spectrometry methods. In the first approach, a chemically stabilized form of Max (Jean-François et al., 2003) in the absence of DNA was subjected to ^{15}N-HSQC in the absence and presence of **KI-MS2-008**, and the change in chemical shift perturbation was quantified. After mapping the structure to the previously published NMR of Max (Sauve et al., 2004), it was revealed that residues L44 and I51 and the surrounding region were most affected by compound treatment, suggesting a possible binding region for **KI-MS2-008** (Figures 3F and S5F). In the second approach, we digested Max samples, one containing the **KI-MS2-085** covalent adduct and one without, and subjected them to liquid chromatography-mass spectrometry analysis (Figures S5A and S5B). Comparative analysis of the two

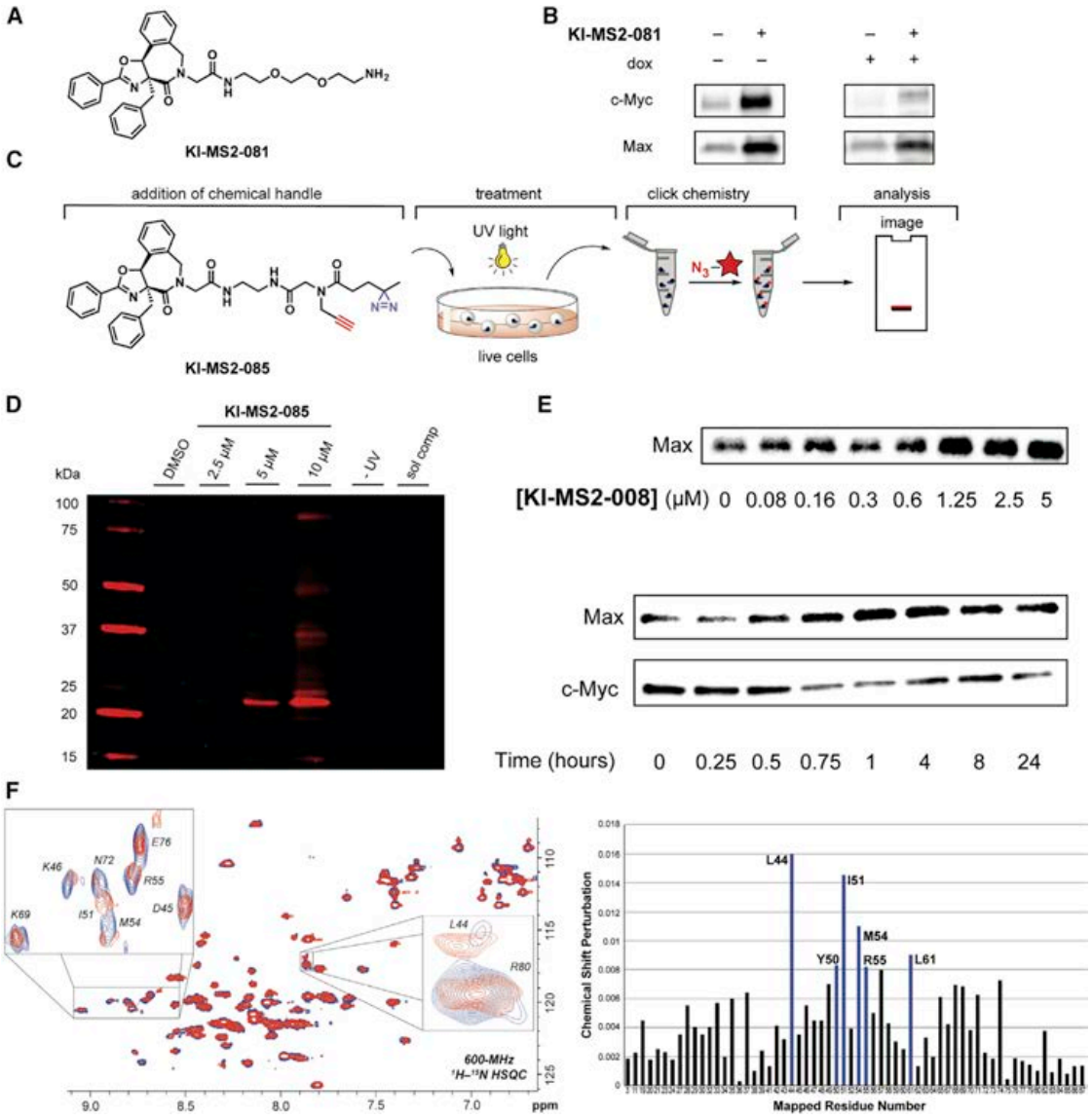

Figure 3. KI-MS2-008 and Analogs Engage Max *In Vitro* and in Live Cells

(A) Chemical structure of **KI-MS2-081** analog containing a primary amine for covalent coupling to NHS-activated magnetic beads.

(B) Immunoblots of Max and c-Myc from samples containing proteins bound to beads with or without **KI-MS2-081** incubated with lysates from P493-6 with and without doxycycline.

(C) Workflow schematic for **KI-MS2-085** analog containing both diazirine and alkyne moieties, enabling crosslinking to targets through the diazirine (in blue) and detection using the alkyne (in red) after copper-catalyzed azide-alkyne cycloaddition to a fluorophore.

(D) Fluorescent gel of proteins labeled by **KI-MS2-085**. P493-6 cells were incubated with 2.5, 5, or 10 μM **KI-MS2-085**. Irradiation of UV light to covalently modify nearby proteins followed by installation of Alexa Fluor 647 allowed visualization of a pair of proteins between 20 and 25 kDa (molecular weight of Max isoforms) on the subsequent gel loaded with labeled lysates.

(E) Immunoblot of Max in soluble fraction using cellular thermal shift assay (CETSA) in intact P493-6 cells following 1 h **KI-MS2-008** dosing treatment (top). Time course of c-Myc and Max protein levels in soluble fraction using CETSA in intact P493-6 cells at 10 μM **KI-MS2-008** visualized by immunoblots (bottom).

(F) ^{15}N-HSQC in the absence (blue) and presence (red) of 150 μM **KI-MS2-008** (left) and the quantification of the change in chemical shift (right).

See also Figure S5.

samples showed a loss of the peptides which contained residues L44 and I51 with **KI-MS2-085** treatment, suggesting formation of the **KI-MS2-085** covalent adduct in this region, thus corroborating the NMR data (Figure S5G). Additional detailed structural biology studies are currently underway to precisely map contacts.

KI-MS2-008 Induces Max/Max Homodimerization

To understand whether **KI-MS2-008** affected the DNA binding functions of Max, we performed electrophoretic mobility shift assays (EMSAs). While a known c-Myc/Max disrupter, 10058-F4 (F4) (Yin et al., 2003), decreased the level of c-Myc/Max heterodimers bound to DNA at active concentrations

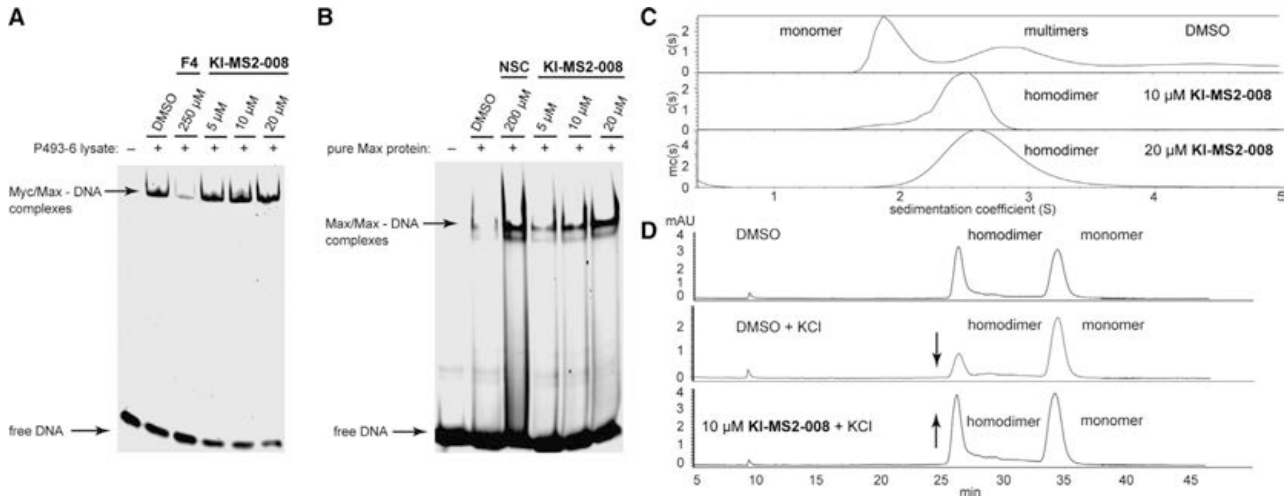

Figure 4. KI-MS2-008 Induces Max/Max Homodimerization

(A) Electrophoretic mobility shift assay (EMSA) utilizing Alexa Fluor 684-labeled E-box DNA incubated with P493-6 lysate treated with 10058-F4 (F4) or **KI-MS2-008**.

(B) EMSA involving pure recombinant Max protein binding to Alexa Fluor 684-labeled E-box DNA incubated with NSC13728 or **KI-MS2-008**.

(C) Plot of the distribution of sedimentation coefficients (c(s)) versus S, calculated from analytical ultracentrifugation sedimentation velocity experiments carried out with untreated Max protein or Max protein treated with 10 and 20 μM **KI-MS2-008**.

(D) Size-exclusion chromatography of pure recombinant Max protein, Max protein with high KCl concentration, and Max protein with high KCl concentration treated with 10 μM **KI-MS2-008**.

See also Figure S5.

reported previously, **KI-MS2-008** (up to 20 μM) had no effect on c-Myc/Max heterodimerization (Figure 4A), consistent with the bead-based pull down from cell lysates. In contrast, **KI-MS2-008** stabilized Max/Max homodimers bound to DNA in a solution containing pure recombinant Max, similarly to the Max/Max homodimer stabilizer NSC13728 (NSC) (Jiang et al., 2009), as visualized and quantified by EMSA (Figures 4B and S5E). The stabilization of the Max/Max homodimer by **KI-MS2-008** was further supported by analytical ultracentrifugation experiments involving pure Max (Figure 4C). Untreated Max protein exhibited two peaks representing the monomer and homodimer, respectively, at a 1.44:1 ratio. Incubation of the protein with 10 or 20 μM **KI-MS2-008** shifted the distribution to predominantly Max/Max homodimers. When fit to a monomer-dimer self-association model (Brautigam, 2011), the data demonstrated a strong enhancement of the Max dimerization affinity in the absence of DNA with **KI-MS2-008** treatment to signify Max/Max homodimer stabilization, which is similar to results observed with NSC13728 (Jiang et al., 2009). Specifically, the data yielded a dimerization affinity K_d value of 8 μM in absence of the compound, which was strongly enhanced to nanomolar affinity (12 nM with 10 μM **KI-MS2-008** and 10 nM with 20 μM **KI-MS2-008**). In addition, size-exclusion chromatography demonstrated an increased concentration of Max/Max homodimer relative to Max monomer after 10 μM **KI-MS2-008** treatment (Figure 4D), further supporting the hypothesis that **KI-MS2-008** stabilizes the Max/Max homodimer.

In P493-6 Cells, KI-MS2-008 Treatment Decreases c-Myc Protein Levels and Causes Global Changes to the Transcriptome that Mimic Myc Inactivation

We next sought to monitor the effects of **KI-MS2-008** at the protein level in P493-6 cells. While Max protein levels were not perturbed, we observed a time-dependent decrease in total c-Myc protein levels, in addition to concomitant decreases in c-Myc protein levels phosphorylated at S62 and T58, on treatment with 10 μM **KI-MS2-008** (Figures 5A and S6A). Decreased c-Myc protein levels were partially rescued when cells were co-treated with 10 μM MG132 (Tsubuki et al., 1996), suggesting a role for proteasome-mediated degradation as one mechanism for alterations in c-Myc protein levels in this cell line (Figure 5B). Similar observations were recently reported for two Myc/Max heterodimer antagonists (Choi et al., 2017; Wang et al., 2015), but increases of ubiquitin-conjugated c-Myc levels were not observed with **KI-MS2-008** treatment (Figure S6B). We did not detect changes in the protein levels of other Max network members such as Mxd1, Mxd4, or Mlx (Ayer et al., 1993; Billin et al., 1999; Conacci-Sorrell et al., 2014) with 10 μM **KI-MS2-008** treatment over 24 h (Figure S6A). Overall, these results suggest that **KI-MS2-008** affects Myc protein levels in P493-6 cells to further promote a shift in equilibrium away from the Myc/Max heterodimer within the dynamic network, although the precise molecular mechanism is still unclear and is the subject of ongoing study.

To understand the impact of **KI-MS2-008** treatment on the global transcriptome and Myc-driven gene expression, we performed RNA sequencing (RNA-seq) experiments in P493-6 cells. A strong correlation was observed between 10 μM **KI-MS2-008** treatment (8 h) and doxycycline addition to turn off c-Myc expression ($r = 0.87$) (Figure 5C). Furthermore, a group of genes regulated by Myc (Liberzon et al., 2015) appeared enriched in the genes downregulated in response to 10 μM **KI-MS2-008** treatment (Figures 5C and S6C). This observation was confirmed using gene set enrichment analysis and extended to other Myc target gene sets (Subramanian et al., 2005) at 1 and 10 μM **KI-MS2-008** (Figures 5D and S6D). In addition, to observe

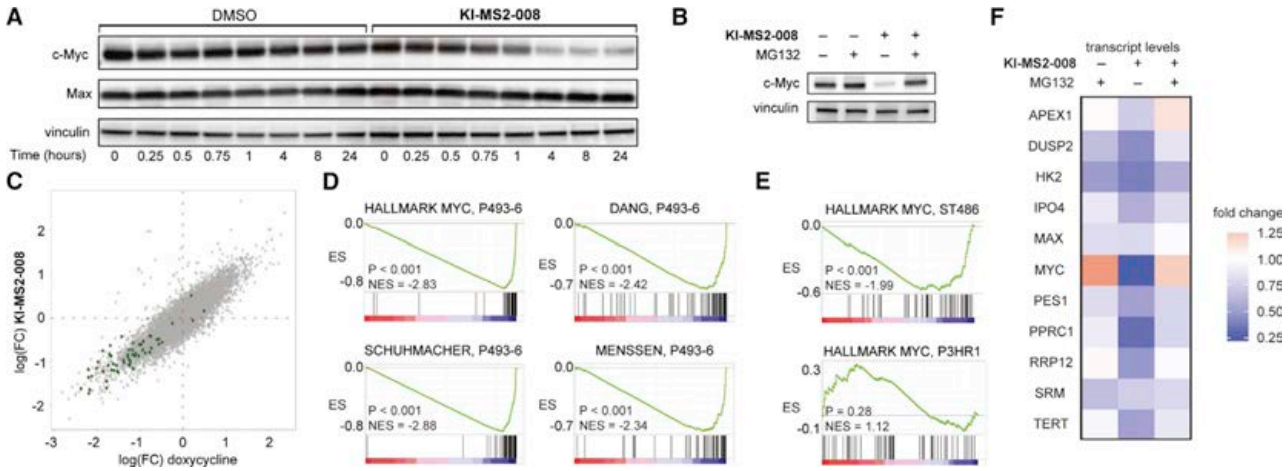

Figure 5. KI-MS2-008 Decreases Myc Protein Levels and Affects the Global Myc Transcriptional Program

(A) Time course of c-Myc and Max protein levels in P493-6 treated with 10 μM **KI-MS2-008** visualized by immunoblots.

(B) c-Myc protein levels with 4 h of 10 μM **KI-MS2-008** and/or proteasome inhibitor MG132 treatment in P493-6 visualized by immunoblots demonstrating partial rescue of c-Myc protein levels.

(C) Scatterplot of RNA-seq data comparing Myc inactivation via doxycycline (8 h) and **KI-MS2-008** treatment in P493-6 cells at 8 h of 10 μM **KI-MS2-008**. Green dots correspond to genes from the HALLMARK_MYC_TARGETS _V2 (HALLMARK MYC) gene set.

(D) Gene set enrichment analysis (GSEA) plots of enrichment scores (ES) corresponding to RNA-seq datasets for P493-6 cells treated with 10 μM **KI-MS2-008** for 8 h with normalized enrichment scores (NES) and nominal p values (n = 4 technical replicates). Four Myc target gene sets are shown.

(E) GSEA plots of ES corresponding to RNA-seq datasets for P3HR1 cells and ST486 cells treated with 10 μM **KI-MS2-008** for 8 h with NES and nominal p values (n = 4 technical replicates). HALLMARK_MYC_TARGETS _V2 (HALLMARK MYC) gene set is shown.

(F) Heatmap showing fold changes in Myc-driven genes in response to 10 μM **KI-MS2-008**, 10 μM MG132, or the combination at 4 h as determined by qPCR (n = 3 technical replicates).

See also Figure S6.

whether the transcriptional effects of **KI-MS2-008** occurred in non-engineered cell lines, we chose to monitor global transcriptional programs in ST486 and P3HR1, which were sensitive and insensitive, respectively, toward both **KI-MS2-001** and **KI-MS2-008** treatment (Figures S1F, S1G, S4C, and S4D). **KI-MS2-008** downregulated c-Myc-regulated genes (Liberzon et al., 2015) in ST486 cells, but this enrichment was not observed in the P3HR1 cells (Figures 5E and S6E). To determine the contribution of c-Myc protein level decreases toward transcriptional repression of Myc-driven genes, we monitored transcript levels of *MYC* and a panel of canonical Myc reporter genes using qPCR. We observed repression of these genes in response to 10 μM **KI-MS2-008** by 2 h and a general reversal of this effect with co-treatment of 10 μM MG132 at 2 and 4 h (Figures 5F and S6F).

KI-MS2-008 Treatment Decreases c-Myc Protein Binding at Promoters of Active Myc-Regulated Genes and Increases Max Protein Binding at the Same Promoters

To determine the effect of **KI-MS2-008** treatment on the global chromatin landscape of Myc and Max, we used chromatin immunoprecipitation sequencing (ChIP-seq) (Lin et al., 2012). We first focused on the 10-kb region surrounding the transcriptional start sites (TSSs) of *NR1D1* and *DDX31* as representative Myc-regulated genes (Altman et al., 2015). Treatment of P493-6 cells with 1 μM **KI-MS2-008** led to decreases in signals of active enhancer marker H3K27ac and c-Myc, as well as substantial increases in Max signal at the core promoters of these genes after 4 and 24 h (Figures 6A and 6B). These perturbations to the TSSs of *NR1D1* and *DDX31* corresponded with decreases in their mRNA levels at 4 and 8 h of compound treatment, with partially recovered levels at 24 h (Figures 6C and 6D). We then extended our analysis to 14,792 active genes (those with H3K27ac at the promoter) and observed similar decreases in H3K27ac signal and c-Myc binding and increases in Max binding at these TSSs (Figures 6E–6G). A comparison of the top 1,000 genes with the strongest signals for c-Myc occupancy, as measured by the area under the curve of c-Myc at the proximal promoter (± 1 kb TSS region) and proximal enhancers (± 50 kb of TSS) with other active genes, revealed significant differences between changes in expression of Myc-regulated genes and other active genes over the 24-h **KI-MS2-008** treatment, suggesting that **KI-MS2-008** can specifically perturb Myc-regulated genes (Figure 6H). Taken together, these results demonstrate a global loss of c-Myc and H3K27ac, and a global stabilization of Max at promoter sites with **KI-MS2-008** treatment, along with downregulation of genes with Myc-occupied TSSs. These results are consistent with previous observations that **KI-MS2-008** stabilizes the Max/Max homodimer and decreases Myc protein levels.

KI-MS2-008 Exhibits Efficacy in Cellular and Murine Cancer Models

To further test the applicability of **KI-MS2-001** and **KI-MS2-008** in a broader spectrum of cancer models, we first evaluated whether these compounds modulated viable cell levels of Myc-driven cancer cell lines derived from tumors of transgenic mouse

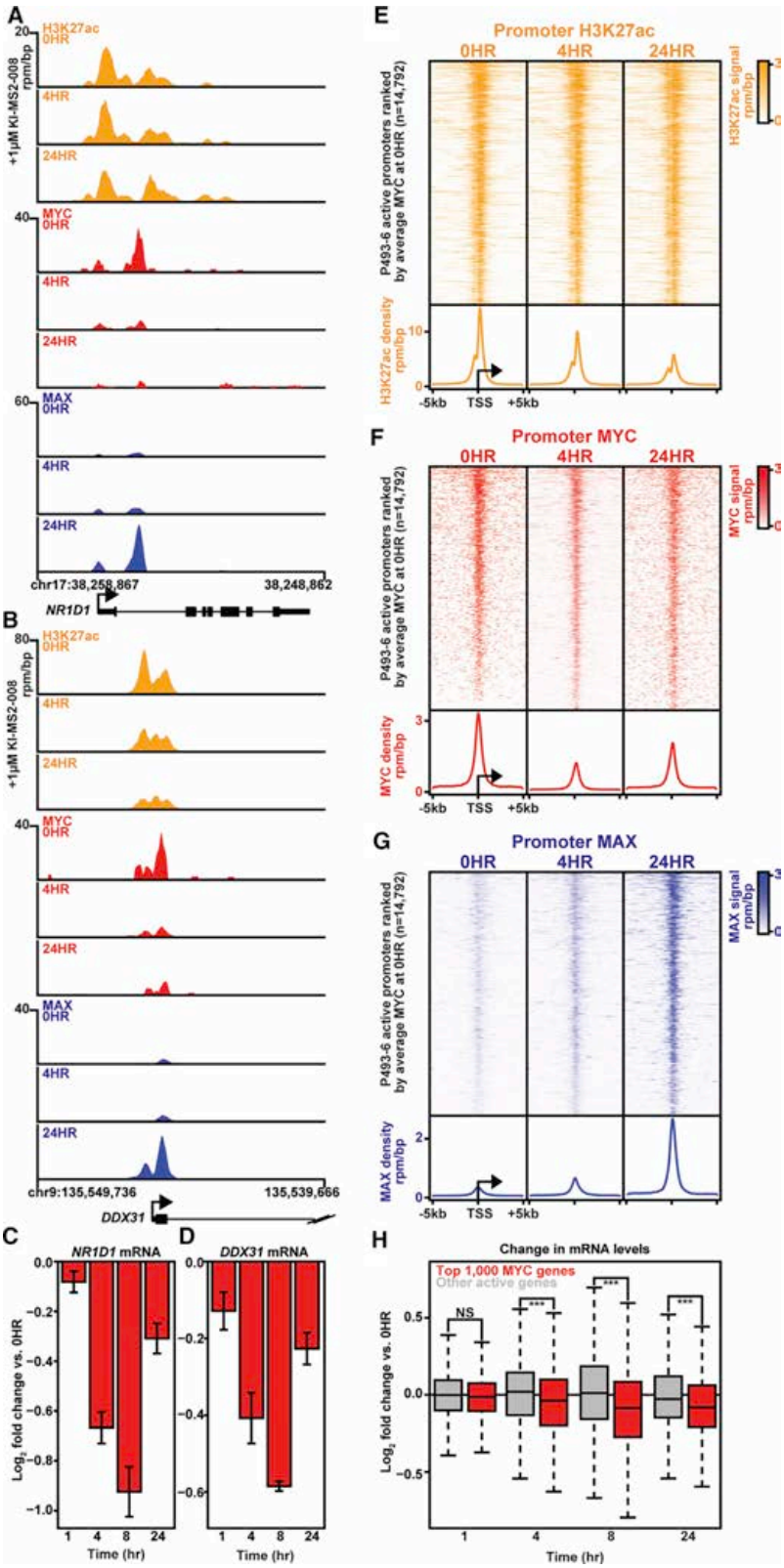

Figure 6. KI-MS2-008 Treatment Decreases c-Myc Protein Binding and Increases Max Protein Binding at Promoters of Myc-Occupied Genes

(A and B) Gene tracks of H3K27ac (gold), c-Myc (red), and Max (blue) binding at 0 h (top), 4 h (middle), and 24 h (bottom) after 1 μM **KI-MS2-008** treatment (n = 1 replicate) at the (A) *NR1D1* gene or (B) *DDX31* gene.

(C and D) Bar graphs of the mean $\log_2$ fold changes (versus 0 h) of the amount of (C) *NR1D1* or (D) *DDX31* mRNA at 1, 4, 8, and 24 h of 1 μM **KI-MS2-008** treatment. Error bars represent the standard deviation of the mean (n = 3 replicates).

(E–G) Heatmap of (E) H3K27ac, (F) c-Myc, and (G) Max levels at transcription start site (TSS) regions at 0, 4, and 24 h of 1 μM **KI-MS2-008** treatment. TSSs for all active promoters in P493-6 cells are shown and ranked by average Myc occupancy at 0 h. Color scaled intensities are in units of rpm/bp (n = 1 replicate).

(H) Boxplots of $\log_2$ fold changes (versus 0 h) of expression of Myc-occupied genes at 1, 4, 8, and 24 h of 1 μM **KI-MS2-008** treatment (n = 3 replicates). The top 1,000 MYC genes based on Myc occupancy at enhancers and promoters are shown in red and other active genes (n = 6,835) in gray. Significance is denoted (Welch's two-tailed t test): ***$p < 1 \times 10^{-9}$, **$p < 1 \times 10^{-6}$.

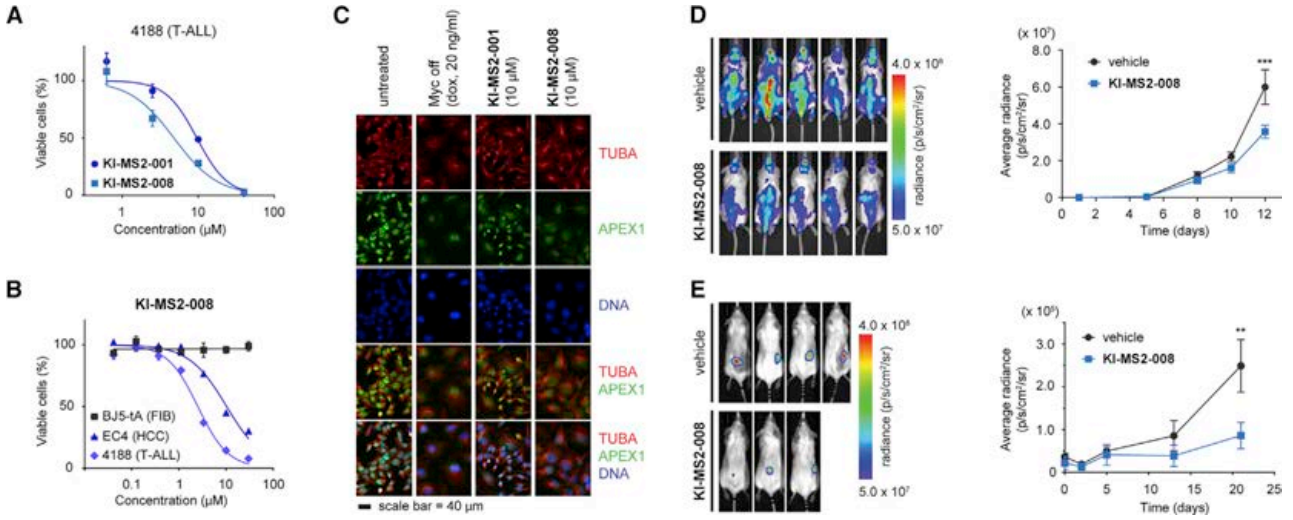

Figure 7. KI-MS2-008 Exhibits Efficacy in Cellular and Murine Cancer Models

(A) Dose-response curves for Myc-driven T-ALL cancer cell line (4188) viable cell levels in response to **KI-MS2-001** or **KI-MS2-008** treatment (n = 3, error bars represent mean ± SEM).

(B) Dose-response curves for Myc-driven murine cancer cell lines (EC4: HCC, 4188: T-ALL), and normal human h-TERT immortalized fibroblasts (BJ5-tA: FIB) viable cell levels in response to **KI-MS2-008** treatment (n = 3, error bars represent mean ± SEM).

(C) Immunofluorescence images of a Myc-driven OS cell line treated with 10 μM **KI-MS2-001**, 10 μM **KI-MS2-008**, or with doxycycline to inactivate Myc expression. α-tubulin and Apex1 were visualized using specific antibodies.

(D) Representative bioluminescence imaging (BLI) of day 12 (left) and data quantitation of BLI time course (right) for NSG mice bearing Myc-driven luciferase-labeled T-ALL treated with vehicle or 0.06 mg/kg **KI-MS2-008** intravenously on days 4–12 (vehicle: n = 6 mice, **KI-MS2-008**: n = 8 mice, error bars represent mean ± SEM).

(E) BLI of day 21 (left) and data quantitation of BLI time course (right) for NSG mice with subcutaneous transplants of Myc-driven luciferase-labeled HCC treated with vehicle or 0.24 mg/kg **KI-MS2-008** intraperitoneally (on days 4–21, 5-on/2-off schedule) (vehicle: n = 4 mice, **KI-MS2-008**: n = 3 mice, error bars represent mean ± SEM). **p < 0.01, ***p < 0.001; two-way ANOVA with p values of Bonferroni post test for treatment endpoints (D and E).

See also Figure S7.

models of Myc-induced T cell acute lymphoblastic leukemia (T-ALL), hepatocellular carcinoma (HCC), and osteosarcoma (OS) (Felsher and Bishop, 1999; Jain et al., 2002; Shachaf et al., 2004). **KI-MS2-008** showed a stronger effect on viable cell levels of Myc-driven T-ALL (4188) compared with **KI-MS2-001** (Figure 7A). **KI-MS2-008** inhibited viable cell levels of lines derived from HCC (EC4) and T-ALL (4188), but **KI-MS2-008** had no effect on normal human fibroblast (BJ5-tA) viable cell levels (Figure 7B). A Myc-driven OS cell line was used to assess the potential of **KI-MS2-001** and **KI-MS2-008** to induce differentiation via Myc inactivation. Morphological changes associated with differentiation were assessed by visualizing α-tubulin, while the expression of a known Myc target, Apex1 (Zeller et al., 2003), was used as a readout for Myc activity. Treatment with 10 μM **KI-MS2-008** resulted in differentiation and downregulation of Apex1 expression, which resulted in indistinguishable immunofluorescence images of cells treated with **KI-MS2-008** from cells in which Myc expression was shut off by doxycycline (Figure 7C). The *in vivo* efficacy of **KI-MS2-008** was then tested in allograft models of Myc-driven T-ALL and HCC. Luciferase-labeled T-ALL cells were injected into NOD/SCID/IL-2Rγ^{null} (NSG) mice intravenously and mice were treated intravenously with vehicle or **KI-MS2-008** (0.06 mg/kg) daily, starting after tumor cell engraftment (day 4). Mice treated with **KI-MS2-008** showed a significant reduction in tumor burden compared with vehicle control-treated mice (Figure 7D). In addition, NSG mice with subcutaneous transplants of Myc-driven HCC cells were treated with intraperitoneal injections of either vehicle or **KI-MS2-008** (0.24 mg/kg) starting after tumor cell engraftment (day 4, 5-on/2-off schedule). Significantly smaller tumors were observed in **KI-MS2-008**-treated mice compared with vehicle-treated control mice (Figure 7E). Following this, the *in vivo* pharmacokinetic properties of **KI-MS2-008** were analyzed by a single high dose (0.731 mg/kg) study in healthy KP53 mice (DuPage et al., 2009) (n = 3), which demonstrated complete clearance from plasma in ~24 h with 50% of the probe being cleared in 30 min, similarly to its metabolic stability in mouse microsomes (Figures S7A–S7C). Repeated doses of **KI-MS2-008** resulted in slightly higher levels in the plasma 24 h after the last dose compared with vehicle control-treated mice, and had no toxic effects on healthy mice over the course of a week, as observed by body weight (Figure S7D), behavior, and H&E stains of the liver and kidney. These results suggest that higher doses would be tolerable for future *in vivo* studies exploring the efficacy of **KI-MS2-008** in a broad swath of cancer models.

DISCUSSION

As Myc requires Max for DNA binding and subsequent transcriptional activation of target genes, a major area of research has focused on disrupting the Myc/Max interaction. These efforts have yielded a number of small molecules to mediate Myc-driven transcription via disruption of this heterodimer, but few have shown efficacy in mouse models (Soodgupta

et al., 2015; Stellas et al., 2014). As an alternative approach, stabilization of the Max/Max homodimer to indirectly target the Myc/Max heterodimer was first explored using virtual ligand screening to predict candidate binders of the Myc/Max and Max/Max dimers, followed by fluorescence resonance energy transfer assays to prioritize Max/Max homodimer stabilizers. This work led to the discovery of NSC13728, a symmetric small molecule that inhibits c-Myc-regulated oncogenic transformation, cell growth, and target gene transcription via Max/Max homodimer stabilization (Jiang et al., 2009). Despite this success, this strategy to indirectly modulate Myc-driven transcription via Max/Max homodimer stabilization has not been as widely explored.

Here we report the discovery of a small molecule with a unique asymmetric scaffold to perturb the balance of Myc/Max and Max/Max dimers. We used mechanistically unbiased binding assays involving SMMs to identify **KI-MS2-001**, a polycyclic lactam that emerged from a library of DOS with a high level of structural diversity (Mitchell and Shaw, 2006). SAR studies led to the synthesis of the analog **KI-MS2-008**, and we demonstrated modulation of Max function by stabilizing the Max/Max homodimer using this compound. **KI-MS2-008** also decreased Myc protein levels, perturbed Myc-driven transcriptional programs, induced Myc-dependent cellular differentiation, and affected viable cell growth of engineered and non-engineered cell lines. We also observed a global loss of c-Myc and a global stabilization of Max at promoter sites with **KI-MS2-008** treatment. Although unoptimized for potency or physicochemical properties, **KI-MS2-008** exhibited preliminary *in vivo* efficacy at low doses by significantly reducing tumor volume in T-ALL and HCC mouse models, although we acknowledge that this study does not assess the effect of **KI-MS2-008** on anti-tumor immunity. With the introduction of **KI-MS2-008**, we provide further support that, by stabilizing the Max homodimer, chemical probes can effectively perturb this dynamic bHLHLZ protein network with overall effects observed in cancer cell lines and mouse models, consistent with Myc modulation.

Several questions related to the molecular and cellular mechanisms of **KI-MS2-008** remain unanswered to date. For example, the precise binding mode of the compound to Max has not been defined, although preliminary NMR and proteomics studies suggest binding to the L44 and I51 residues and the surrounding region. Detailed investigations involving multiple structural biology approaches are currently underway in our labs. We have not yet precisely characterized the mechanisms by which Myc protein levels and Myc-regulated transcript levels are decreased when the dynamic equilibrium of Myc/Max heterodimer or Max/Max homodimer is perturbed (e.g., possibly selective degradation of Myc in the nucleolus and/or differential gene regulation by Myc) (Amati and Sanchez-Arévalo Lobo, 2007; Kress et al., 2015). We also have yet to understand how **KI-MS2-008** perturbs the wider Max interactome. Despite these outstanding questions, **KI-MS2-008** can serve as a useful tool for interrogating the roles of Max in transcription and cell biology, as well as understanding the importance of Max dimerization status in cancer and other disease settings. Moving forward, the compound may also serve as a scaffold for a next generation of Max-directed chemical probes.

SIGNIFICANCE

The bHLHLZ protein network—including Myc, Max, and Mxd—has crucial roles in normal cellular processes such as cell proliferation, metabolism, apoptosis, and differentiation, but its activity is deregulated in a majority of human cancers. Despite this importance, there is still limited availability of high-quality chemical tools to investigate this network. Both the Myc/Max and Max/Max dimers bind to the canonical E-box (CACGTC) with the heterodimer activating transcription, while the homodimer competes for the same genomic target sites to attenuate Myc-driven programs. An emerging hypothesis is that the tumor suppressor activity of Max relies on its ability to modulate Myc-driven programs via the homodimer. As such, we have explored alternative modes of Myc perturbation by modulating Max with small molecules, utilizing the mechanistically unbiased SMM to help discover KI-MS2-008. We determined that KI-MS2-008 stabilizes the Max/Max homodimer while also decreasing Myc protein levels and effectively perturbing Myc-driven transcriptional programs. To our knowledge, KI-MS2-008 is the first Max-directed probe to demonstrate *in vivo* efficacy, and the unoptimized probe may serve as a starting point for the development of improved compounds to enable translational studies and to further clarify the relevance of Max as a therapeutic target.

STAR★METHODS

Detailed methods are provided in the online version of this paper and include the following:

- KEY RESOURCES TABLE
- CONTACT FOR REAGENT AND RESOURCE SHARING
- EXPERIMENTAL MODEL AND SUBJECT DETAILS
  - Animal Studies
  - Cell Lines
- METHOD DETAILS
  - Chemical Synthesis
  - Small Molecule Microarray
  - Transcriptional Reporter Assay
  - Viable Cell Assay
  - Flow Cytometry
  - Bead-Based Lysate Pull-down with KI-MS2-081
  - *In Vitro* Labeling of Max with KI-MS2-085
  - Live-Cell Pull-down with KI-MS2-085
  - Electrophoretic Mobility Shift Assay
  - Analytical Ultracentrifugation
  - Size Exclusion Chromatography
  - Cellular Thermal Shift Assay (Molina et al., 2013)
  - ^{15}N-Heteronuclear Single Quantum Coherence
  - Time Course of Protein Levels
  - RNA-seq
  - qPCR
  - Primers for qPCR
  - Ubiquitination Assay
  - Protein Binding Assay
  - Solubility of KI-MS2-001 in Aqueous Buffers
  - Bidirectional Permeability of KI-MS2-001

SUPPLEMENTAL INFORMATION

Supplemental Information includes seven figures and one table and can be found with this article online at https://doi.org/10.1016/j.chembiol.2019.02.009.

ACKNOWLEDGMENTS

The authors thank S. Doyle for critical reading of the manuscript. We also thank J. Bradner, R. Eisenman, T. Golub, S. Levine, M. Schenone, R. Sears, F. White, O. Witte, and R. Young for helpful discussions. We thank D. Eick for P493-6 cells, O. McPherson for SMM technical support, and E. Richards for qPCR support. We apologize to colleagues not cited due to limited space. We thank the Koch Institute Swanson Biotechnology Center for technical support, specifically the Animal Imaging and Preclinical Testing Facility, the Flow Cytometry Facility, the Genomics Core Facility, the Biopolymers & Proteomics Core facility, and the High-Throughput Screening Facility. The project benefitted from the Biophysical Instrumentation and Department of Chemistry Instrumentation facilities at MIT as well as the Center for Science of Therapeutics at the Broad Institute. Bioluminescence imaging was performed in the SCi3 Stanford Small Animal Imaging Service Center. This work was financially supported by the National Cancer Institute through R01-CA160860 (to A.N.K.), P30-CA14051 (Koch Institute Cancer Center Support Core grant), U01-CA176152 (Broad Institute Cancer Target Discovery and Development Center), and NIH/NCI CA170378PQ2 (to D.W.F.), and 1U01CA188383-01/S1 (to D.W.F.). The work was also supported in part by the Leukemia & Lymphoma Society, the Ono Pharma Foundation, the MIT Deshpande Center for Technological Innovation, the MIT Center for Precision Cancer Medicine, the AACR-Bayer Innovation and Discovery Grant, and the Merkin Institute Fellows Program at the Broad Institute (to A.N.K.). C.Y.L is supported by the Cancer Prevention Research Institute of Texas (RR150093), the NIH, and NCI (1R01CA215452-01), and is a Pew-Stewart Scholar for Cancer Research (Alexander and Margaret Stewart Trust). N.B.S. is supported by the GSK-MIT Gertrude B. Elion Research Fellowship Program for Drug Discovery and Disease and the Ludwig Center Fund at MIT. A.C. is supported by a Koch Institute Graduate Fellowship in Cancer Research. A.D. is supported by a Lymphoma Research Foundation Postdoctoral Fellowship. H.L.E is supported by a Koch Institute Quinquennial Cancer Research Fellowship. R.M.W. is supported by a Ludwig Center for Molecular Oncology Graduate Fellowship.

AUTHOR CONTRIBUTIONS

N.B.S., A.C., A.D., R.M.W., M.A.R., T.L., F.C., M.H.E.W., A.V., C.Y.L., D.W.F., and A.N.K. designed the experiments and analyzed the data. N.B.S., A.C., R.M.W., F.C., M.S.P., M.McM., S.M., H.T., K.R.F., D.B.F., P.A.C., B.L.E., and A.N.K. performed and analyzed screening assays. A.D. and D.W.F. performed cell culture and mouse experiments. E.S., H.L.E., B.H.C., and T.A.L. synthesized small molecules. M.S.P., D.B.F., and B.H.C. analyzed NMR studies. M.A.R. and T.L. performed ChIP-seq and RNA-seq experiments. A.C. and N.B.S. performed target engagement studies. N.B.S. performed mechanistic studies. A.C. and R.M.W. performed RNA-seq sample processing. R.M.W. performed RNA-seq analysis. V.L.B. and S.S.L. sequenced RNA transcripts. S.E. and S.E.M. performed pharmacokinetic studies. D.V.N., C.F., and J.A.H. performed preliminary experiments that initiated the study. B.L.E., D.W.F., and A.N.K. supervised the study. N.B.S., A.C., and A.N.K. wrote the manuscript with input from all authors.

DECLARATION OF INTERESTS

A.N.K. is a founder of Kronos Bio and a member of its scientific advisory board. N.B.S., A.C., E.S., H.L.E., F.C., D.V.N., and A.N.K. have a patent related to this work that is licensed by Kronos Bio. D.W.F. and C.Y.L. are consultants to Kronos Bio.

Received: June 15, 2018
Revised: November 27, 2018
Accepted: February 7, 2019
Published: March 14, 2019

REFERENCES

Altman, Brian J., Hsieh, Annie L., Sengupta, A., Krishnanaiah, Saikumari Y., Stine, Zachary E., Walton, Zandra E., Gouw, Arvin M., Venkataraman, A., Li, B., Goraksha-Hicks, P., et al. (2015). MYC disrupts the circadian clock and metabolism in cancer cells. Cell Metab. *22*, 1009–1019.

Amati, B., and Sanchez-Arévalo Lobo, V.J. (2007). MYC degradation: deubiquitinating enzymes enter the dance. Nat. Cell Biol. *9*, 729–731.

Anders, S., and Huber, W. (2010). Differential expression analysis for sequence count data. Genome Biol. *11*, R106.

Ayer, D.E., Kretzner, L., and Eisenman, R.N. (1993). Mad: a heterodimeric partner for Max that antagonizes Myc transcriptional activity. Cell *72*, 211–222.

Benjamini, Y., and Hochberg, Y. (1995). Controlling the false discovery rate - a practical and powerful approach to multiple testing. J. R. Stat. Soc. Series B Stat. Methodol. *57*, 289–300.

Billin, A.N., Eilers, A.L., Queva, C., and Ayer, D.E. (1999). Mlx, a novel max-like BHLHZip protein that interacts with the max network of transcription factors. J. Biol. Chem. *274*, 36344–36350.

Blackwell, T.K., Kretzner, L.F., Blackwood, E.M., Eisenman, R.N., and Weintraub, H. (1990). Sequence-specific DNA binding by the c-Myc protein. Science *23*, 1149–1151.

Blencowe, A., and Hayes, W. (2005). Development and application of diazirines in biological and synthetic macromolecular systems. Soft Matter. *1*, 178.

Brautigam, C.A. (2011). Using Lamm-equation modeling of sedimentation velocity data to determine the kinetic and thermodynamic properties of macromolecular interactions. Methods *54*, 4–15.

Calderon, M.R., Verway, M., An, B.S., DiFeo, A., Bismar, T.A., Ann, D.K., Martignetti, J.A., Shalom-Barak, T., and White J, H. (2012). Ligand-dependent corepressor (LCoR) recruitment by Kruppel-like factor 6 (KLF6) regulates expression of the cyclin-dependent kinase inhibitor CDKN1A gene. J. Biol. Chem. *287*, 8662–8674.

Cascón, A., and Robledo, M. (2012). MAX and MYC: a heritable breakup. Cancer Res. *72*, 3119–3124.

Champely, S. (2018). pwr: basic functions for power analysis. R package version 1.2-2, https://CRAN.R-project.org/package=pwr.

Choi, S.H., Mahankali, M., Lee, S.J., Hull, M., Petrassi, H.M., Chatterjee, A.K., Schultz, P.G., Jones, K.A., and Shen, W. (2017). Targeted disruption of Myc-Max oncoprotein complex by a small molecule. ACS Chem. Biol. *17*, 2715–2719.

Clemons, P.A., Bodycombe, N.E., Carrinski, H.A., Wilson, J.A., Shamji, A.F., Wagner, B.K., Koehler, A.N., and Schreiber, S.L. (2010). Small molecules of different origins have distinct distributions of structural complexity that correlate with protein-binding profiles. Proc. Natl. Acad. Sci. U S A *107*, 18787–18792.

Conacci-Sorrell, M., McFerrin, L., and Eisenman, R.N. (2014). An overview of MYC and its interactome. Cold Spring Harb. Perspect. Med. *4*, a014357.

Cook, R.D. (1977). Detection of influential observation in linear regression. Technometrics *19*, 15–18.

Dang, C.V. (2012). MYC on the path to cancer. Cell *149*, 22–35.

Darnell, J.E., Jr. (2002). Transcription factors as targets for cancer therapy. Nat. Rev. Cancer *2*, 740–749.

Derr, A., Yang, C., Zilionis, R., Sergushichev, A., Blodgett, D.M., Redick, S., Bortell, R., Luban, J., Harlan, D.M., Kadener, S., et al. (2016). End Sequence Analysis Toolkit (ESAT) expands the extractable information from single-cell RNA-seq data. Genome Res. *26*, 1397–1410.

Devgan, V., Harris, A., Jiang, Q., and Pattison, S. (2012). Cignal reporter assay kit: a high-performance tool for assessing the functions of genes, biologics, and small molecule compounds. https://www.qiagen.com/fi/resources/download.aspx?id=6fc8144b-010b-43d8-9125-bf541a5d9c9c&lang=en.

DuPage, M., Dooley, A.L., and Jacks, T. (2009). Conditional mouse lung cancer models using adenoviral or lentiviral delivery of Cre recombinase. Nat. Protoc. *4*, 1064–1072.

Farrell, A.S., and Sears, R.C. (2014). MYC degradation. Cold Spring Harb. Perspect. Med. *4*, a014365.

Felsenstein, K.M., Saunders, L.B., Simmons, J.K., Leon, E., Calabrese, D.R., Zhang, S., Michalowski, A., Gareiss, P., Mock, B.A., and Schneekloth, J.S. (2016). Small molecule microarrays enable the identification of a selective, Quadruplex-binding inhibitor of MYC expression. ACS Chem. Biol. *11*, 139–148.

Felsher, D.W. (2010). MYC inactivation elicits oncogene addiction through both tumor cell-intrinsic and host-dependent mechanisms. Genes Cancer *1*, 597–604.

Felsher, D.W., and Bishop, J.M. (1999). Reversible tumorigenesis by MYC in hematopoietic lineages. Mol. Cell *4*, 199–207.

Gabay, M., Li, Y., and Felsher, D.W. (2014). MYC activation is a hallmark of cancer initiation and maintenance. Cold Spring Harb. Perspect. Med. *4*, a014241.

Grzesiek, S., and Bax, A. (1993). The importance of not saturating water in protein NMR. Application to sensitivity enhancement and NOE measurements. J. Am. Chem. Soc. *115*, 12593–12594.

Hart, J.R., Garner, A.L., Yu, J., Ito, Y., Sun, M., Ueno, L., Rhee, J.-K., Baksh, M.M., Stefan, E., Hartl, M., et al. (2014). Inhibitor of MYC identified in a Kröhnke pyridine library. Proc. Natl. Acad. Sci. U S A *111*, 12556–12561.

Hong, J.A., Neel, D.V., Wassaf, D., Caballero, F., and Koehler, A.N. (2014). Recent discoveries and applications involving small-molecule microarrays. Curr. Opin. Chem. Biol. *18*, 21–28.

Hopewell, R., and Ziff, E.B. (1995). The nerve growth factor-responsive PC12 cell line does not express the Myc dimerization partner Max. Mol. Cell. Biol. *15*, 3470–3478.

Jafari, R., Almqvist, H., Axelsson, H., Ignatushchenko, M., Lundback, T., Nordlund, P., and Martinez Molina, D. (2014). The cellular thermal shift assay for evaluating drug target interactions in cells. Nat. Protoc. *9*, 2100–2122.

Jain, M., Arvanitis, C., Chu, K., Dewey, W., Leonhardt, E., Trinh, M., Sundberg, C.D., Bishop, J.M., and Felsher, D.W. (2002). Sustained loss of a neoplastic phenotype by brief inactivation of MYC. Science *297*, 102–104.

Jean-François, N., Frédéric, G., Raymund, W., Benoit, C., and Lavigne, P. (2003). Improving the thermodynamic stability of the leucine zipper of max increases the stability of its b-HLH-LZ: E-box complex. J. Mol. Biol. *326*, 1577–1595.

Jiang, H., Bower, K.E., Beuscher, A.E.t., Zhou, B., Bobkov, A.A., Olson, A.J., and Vogt, P.K. (2009). Stabilizers of the Max homodimer identified in virtual ligand screening inhibit Myc function. Mol. Pharmacol. *76*, 491–502.

Kay, L., Keifer, P., and Saarinen, T. (1992). Pure absorption gradient enhanced heteronuclear single quantum correlation spectroscopy with improved sensitivity. J. Am. Chem. Soc. *114*, 10663–10665.

Koehler, A.N. (2010). A complex task? Direct modulation of transcription factors with small molecules. Curr. Opin. Chem. Biol. *14*, 331–340.

Kress, T.R., Sabò, A., and Amati, B. (2015). MYC: connecting selective transcriptional control to global RNA production. Nat. Rev. Cancer *15*, 593–607.

Laherty, C.D., Yang, W.-M., Sun, J.-M., Davie, J.R., Seto, E., and Eisenman, R.N. (1997). Histone deacetylases associated with the mSin3 corepressor mediate mad transcriptional repression. Cell *89*, 349–356.

Langmead, B., Trapnell, C., Pop, M., and Salzberg, S.L. (2009). Ultrafast and memory-efficient alignment of short DNA sequences to the human genome. Genome Biol. *10*, R25.

Li, H., Handsaker, B., Wysoker, A., Fennell, T., Ruan, J., Homer, N., Marth, G., Abecasis, G., and Durbin, R. (2009). The sequence alignment/map format and SAMtools. Bioinformatics *25*, 2078–2079.

Liberzon, A., Birger, C., Thorvaldsdottir, H., Ghandi, M., Mesirov, J.P., and Tamayo, P. (2015). The Molecular Signatures Database (MSigDB) hallmark gene set collection. Cell Syst. *1*, 417–425.

Lin, C.Y., Loven, J., Rahl, P.B., Paranal, R.M., Burge, C.B., Bradner, J.E., Lee, T.I., and Young, R.A. (2012). Transcriptional amplification in tumor cells with elevated c-Myc. Cell *151*, 56–67.

Livak, K.J., and Schmittgen, T.D. (2001). Analysis of relative gene expression data using real-time quantitative PCR and the 2(-Delta Delta C(T)) method. Methods *25*, 402–408.

Love, M.I., Huber, W., and Anders, S. (2014). Moderated estimation of fold change and dispersion for RNA-seq data with DESeq2. Genome Biol. *15*, 550.

Lu, T.Y., Lu, R.M., Liao, M.Y., Yu, J., Chung, C.H., Kao, C.F., and Wu, H.C. (2010). Epithelial cell adhesion molecule regulation is associated with the maintenance of the undifferentiated phenotype of human embryonic stem cells. J. Biol. Chem. *285*, 8719–8732.

Mackinnon, A.L., and Taunton, J. (2009). Target identification by diazirine photo-cross-linking and click chemistry. Curr. Protoc. Chem. Biol. *1*, 55–73.

McKeown, M.R., and Bradner, J.E. (2014). Therapeutic strategies to inhibit MYC. Cold Spring Harb. Perspect. Med. *4*, https://doi.org/10.1101/cshperspect.a014266.

Mitchell, J.M., and Shaw, J.T. (2006). A structurally diverse library of polycyclic lactams resulting from systematic placement of proximal functional groups. Angew. Chem. Int. Ed. *45*, 1722–1726.

Molina, D.M., Jafari, R., Ignatushchenko, M., Seki, T., Larsson, E.A., Dan, C., Sreekumar, L., Cao, Y., and Nordlund, P. (2013). Monitoring drug target engagement in cells and tissues using the cellular thermal shift assay. Science *341*, 84–87.

Nair, S.K., and Burley, S.K. (2003). X-ray structures of Myc-Max and Mad-Max recognizing DNA. Cell *112*, 193–205.

Pajic, A., Spitkovsky, D., Christoph, B., Kempkes, B., Schuhmacher, M., Staege, M.S., Brielmeier, M., Ellwart, J., Kohlhuber, F., Bornkamm, G.W., et al. (2000). Cell cycle activation by c-myc in a Burkitt lymphoma model cell line. Int. J. Cancer *87*, 787–793.

Palmer, A.G., Cavanagh, J., Wright, P.E., and Rance, M. (1991). Sensitivity improvement in proton-detected two-dimensional heteronuclear correlation NMR spectroscopy. J. Magn. Reson. *93*, 151–170.

Pop, M.S., Stransky, N., Garvie, C.W., Theurillat, J.P., Hartman, E.C., Lewis, T.A., Zhong, C., Culyba, E.K., Lin, F., Daniels, D.S., et al. (2014). A small molecule that binds and inhibits the ETV1 transcription factor oncoprotein. Mol. Cancer Ther. *13*, 1492–1502.

Riss, T.L., Moravec, R.A., Niles, A.L., Duellman, S., Benink, H.A., Worzella, T.J., and Minor, L. (2013). Cell Viability Assays (Eli Lilly & Company and the National Center for Advancing Translational Sciences).

Sauve, S., Tremblay, L., and Lavigne, P. (2004). The NMR solution structure of a mutant of the Max b/HLH/LZ free of DNA: insights into the specific and reversible DNA binding mechanism of dimeric transcription factors. J. Mol. Biol. *342*, 813–832.

Schleucher, J., Schwendinger, M., Sattler, M., Schmidt, P., Schedletzky, O., Glaser, S.J., Sørensen, O.W., and Griesinger, C. (1994). A general enhancement scheme in heteronuclear multidimensional NMR employing pulsed field gradients. J. Biomol. NMR *4*, 301–306.

Schneider, C.A., Rasband, W.S., and Eliceiri, K.W. (2012). NIH image to imageJ: 25 years of image analysis. Nat. Methods *9*, 671–675.

Schuhmacher, M., Staege, M.S., Pajic, A., Polack, A., Weidle, U.H., Bornkamm, G.W., Eick, D., and Kohlhuber, F. (1999). Control of cell growth by c-Myc in the absence of cell division. Curr. Biol. *9*, 1255–1258.

Shachaf, C.M., Kopelman, A.M., Arvanitis, C., Karlsson, Å., Beer, S., Mandl, S., Bachmann, M.H., Borowsky, A.D., Ruebner, B., Cardiff, R.D., et al. (2004). MYC inactivation uncovers pluripotent differentiation and tumour dormancy in hepatocellular cancer. Nature *431*, 1112.

Smith, E., and Collins, I. (2015). Photoaffinity labeling in target- and binding-site identification. Future Med. Chem. *7*, 159–183.

Soodgupta, D., Pan, D., Cui, G., Senpan, A., Yang, X., Lu, L., Weilbaecher, K.N., Prochownik, E.V., Lanza, G.M., and Tomasson, M.H. (2015). Small molecule MYC inhibitor conjugated to integrin-targeted nanoparticles extends survival in a mouse model of disseminated multiple myeloma. Mol. Cancer Ther. *14*, 1286–1294.

Soucek, L., Jucker, R., Panacchia, L., Ricordy, R., Tatò, F., and Nasi, S. (2002). Omomyc, a potential Myc dominant negative, enhances Myc-induced apoptosis. Cancer Res. *62*, 3507–3510.

Soucek, L., Whitfield, J., Martins, C.P., Finch, A.J., Murphy, D.J., Sodir, N.M., Karnezis, A.N., Swigart, L.B., Nasi, S., and Evan, G.I. (2008). Modelling Myc inhibition as a cancer therapy. Nature *455*, 679–683.

Soumillon, M., Cacchiarelli, D., Semrau, S., van Oudenaarden, A., and Mikkelsen, T.S. (2014). Characterization of directed differentiation by high-throughput single-cell RNA-Seq. bioRxiv. https://doi.org/10.1101/003236.

Speers, A.E., and Cravatt, B.F. (2009). Activity-based protein profiling (ABPP) and click chemistry (CC)-ABPP by MudPIT mass spectrometry. Curr. Protoc. Chem. Biol. *1*, 29–41.

Stanton, B.Z., Peng, L.F., Maloof, N., Nakai, K., Wang, X., Duffner, J.L., Taveras, K.M., Hyman, J.M., Lee, S.W., Koehler, A.N., et al. (2009). A small molecule that binds Hedgehog and blocks its signaling in human cells. Nat. Chem. Biol. *5*, 154–156.

Stellas, D., Szabolcs, M., Koul, S., Li, Z., Polyzos, A., Anagnostopoulos, C., Cournia, Z., Tamvakopoulos, C., Klinakis, A., and Efstratiadis, A. (2014). Therapeutic effects of an anti-Myc drug on mouse pancreatic cancer. J. Natl. Cancer Inst. *106*, https://doi.org/10.1093/jnci/dju320.

Subramanian, A., Tamayo, P., Mootha, V.K., Mukherjee, S., Ebert, B.L., Gillette, M.A., Paulovich, A., Pomeroy, S.L., Golub, T.R., Lander, E.S., et al. (2005). Gene set enrichment analysis: a knowledge-based approach for interpreting genome-wide expression profiles. Proc. Nat. Acad. Sci. U S A *102*, 15545–15550.

Tsubuki, S., Saito, Y., Tomioka, M., Ito, H., and Kawashima, S. (1996). Differential inhibition of calpain and proteasome activities by peptidyl aldehydes of Di-leucine and Tri-leucine. J. Biochem. *119*, 572–576.

Vegas, A.J., Fuller, J.H., and Koehler, A.N. (2008). Small-molecule microarrays as tools in ligand discovery. Chem. Soc. Rev. *37*, 1385–1394.

Wang, H., Teriete, P., Hu, A., Raveendra-Panickar, D., Pendelton, K., Lazo, J.S., Eiseman, J., Holien, T., Misund, K., Oliynyk, G., et al. (2015). Direct inhibition of c-Myc-Max heterodimers by celastrol and celastrol-inspired triterpenoids. Oncotarget *6*, 32380–32395.

Yin, X., Giap, C., Lazo, J.S., and Prochownik, E.V. (2003). Low molecular weight inhibitors of Myc-Max interaction and function. Oncogene *22*, 6151–6159.

Zeller, K.I., Jegga, A.G., Aronow, B.J., O'Donnell, K.A., and Dang, C.V. (2003). An integrated database of genes responsive to the Myc oncogenic transcription factor: identification of direct genomic targets. Genome Biol. *4*, R69.

Zhang, Y., Liu, T., Meyer, C.A., Eeckhoute, J., Johnson, D.S., Bernstein, B.E., Nusbaum, C., Myers, R.M., Brown, M., Li, W., et al. (2008). Model-based analysis of ChIP-seq (MACS). Genome Biol. *9*, R137.

STAR★METHODS

KEY RESOURCES TABLE

REAGENT or RESOURCE	SOURCE	IDENTIFIER
Antibodies		
Mouse monoclonal Alexa Fluor® 647-conjugated anti-His5	Qiagen	Cat#35370
Mouse monoclonal anti-c-Myc (9E10)	Santa Cruz Biotechnology	Cat#sc-40; RRID: AB_627268
Rabbit polyclonal anti-c-Myc (N-262)	Santa Cruz Biotechnology	Cat#sc-764; RRID: AB_631276
Mouse monoclonal anti-c-Myc (9E11)	Abcam	Cat#ab56; RRID: AB_304976
Rabbit IgG control	Santa Cruz Biotechnology	Cat#sc-2027; RRID: AB_737197
Rabbit polyclonal anti-Max (C-124)	Santa Cruz Biotechnology	Cat#sc-765; RRID: AB_2281780
Goat polyclonal anti-Max	Abcam	Cat#ab9700; RRID: AB_2141674
Rabbit monoclonal anti-Max	Abcam	Cat#ab199489
Rabbit polyclonal anti-Max (C-17)	Santa Cruz Biotechnology	Cat#sc-197, lot C3016; RRID: AB_2281783
Horse anti-mouse IgG, HRP-linked	Cell Signaling Technology	Cat#7076; RRID: AB_330924
Goat anti-rabbit IgG, HRP-linked	Cell Signaling Technology	Cat#7074; RRID: AB_2099233
Rabbit polyclonal anti-c-Myc (pT58)	Abcam	Cat#ab28842; RRID: AB_731667
Mouse monoclonal anti-c-Myc (pS62)	Abcam	Cat#ab78318; RRID: AB_1566069
Mouse monoclonal anti-MLX (F-12)	Santa Cruz Biotechnology	Cat#sc-393086
Mouse monoclonal anti-Mxd1 (F-1)	Santa Cruz Biotechnology	Cat#sc-8012; RRID: AB_627900
Goat polyclonal anti-Mxd4 (N-19)	Santa Cruz Biotechnology	Cat#sc-1221; RRID: AB_2235630
Mouse anti-ubiquitin (FK2)	Enzo Life Sciences	BML-PW8810; RRID: AB_10541840
Mouse monoclonal anti-vinculin (hVIN-1)	Sigma-Aldrich	Cat#V9131; RRID: AB_477629
Mouse monoclonal anti-tubulin (DM1A)	Sigma-Aldrich	Cat#T9026; RRID: AB_477593
Rabbit polyclonal anti-Apex1	Cell Signaling Technology	Cat#4128S; RRID: AB_2057933
Goat polyclonal IRDye® 800CW anti-Rabbit IgG	LICOR	Cat#925-32211; RRID: AB_2651127
Goat polyclonal anti-rabbit Alexa Fluor-546	Thermo Fisher Scientific	Cat#A-11035; RRID: AB_2534093
Goat polyclonal anti-mouse Alexa Fluor-647	Thermo Fisher Scientific	Cat#A-21236; RRID: AB_2535805
Rabbit polyclonal to Histone H3 (acetyl K27)	Abcam	Cat#ab4729; RRID: AB_2118291
Chemicals, Peptides, and Recombinant Proteins		
His6-tagged recombinant Max protein	Panomics	Cat#RP0080
Recombinant human Max protein	Abcam	Cat#ab95309
NSC13728	Resynthesized in the Koehler lab.	N/A
10058-F4	SigmaAldrich	Cat#F3680-5MG
Critical Commercial Assays		
Cignal Myc Reporter Assay Kit (LUC)	Qiagen	Cat#CCS-012L
Dual-Glo® Luciferase Assay System	Promega	Cat#E2940
CellTiter-Glo® Luminenscent Cell Viability Assay	Promega	Cat#G7572
Aurum™ Total RNA Mini Kit	BioRad	Cat#7326820
Deposited Data		
Small molecule microarray datasets	Clemons et al., 2010, 18787-18792.1125.0116 (DIV06) and 1125.0117 (NPC)	http://chembank.broadinstitute.org/protein/view-protein.htm?id=5000358
RNA-seq dataset	This paper. NCBI GEO: GSE107222	https://www.ncbi.nlm.nih.gov/geo/
ChIP-seq dataset	This paper. NCBI GEO: GSE125863	https://www.ncbi.nlm.nih.gov/geo/

(*Continued on next page*)

Continued

REAGENT or RESOURCE	SOURCE	IDENTIFIER
Experimental Models: Cell Lines		
Human: P493-6	Laboratory of D. Eick	N/A
Human: HEK293T (female)	ATCC	Cat#CRL-3216; RRID: CVCL_0063
Rat: PC12 (male)	ATCC	Cat#CRL-1721; RRID:CVCL_0481
Human: ST-486 (female)	ATCC	Cat#CRL-1647; RRID:CVCL_1712
Human: HL-60 (female)	ATCC	Cat#CCL-240; RRID:CVCL_0002
Human: CA46 (male)	ATCC	Cat#CRL-1648; RRID:CVCL_1101
Human: P3HR1 (male)	ATCC	Cat#HTB-62; RRID:CVCL_2676
Human: SKNMC (female)	ATCC	Cat#HTB-10; RRID:CVCL_0530
Human: U87-MG (male)	ATCC	Cat#HTB-14; RRID:CVCL_0022
Human: T98G (male)	ATCC	Cat#CRL-1690; RRID:CVCL_0556
Human: NCI-H1963 (male)	ATCC	Cat#CRL-5982; RRID:CVCL_1510
Human: NCI-H446 (male)	ATCC	Cat#HTB-171; RRID:CVCL_1562
Human: NCI-H82 (male)	ATCC	Cat#HTB-175; RRID:CVCL_1591
Human: SNU-398 (male)	ATCC	Cat#CRL-2233; RRID:CVCL_0077
Human: PSN-1 (male)	ATCC	Cat#CRM-CRL-3211; RRID:CVCL_1644
Human: COLO-320 (female)	ATCC	Cat#CCL-220; RRID:CVCL_0219
Human: HCC-1599 (female)	ATCC	Cat#CRL-2331; RRID:CVCL_1256
Human: SNU-16 (female)	ATCC	Cat#CRL-5974; RRID:CVCL_0076
Human: NCI-H929 (female)	ATCC	Cat#CRL-9068; RRID:CVCL_1600
Human: MSTO-211H (male)	ATCC	Cat#CRL-2081; RRID:CVCL_1430
Human: DU145 (male)	ATCC	Cat#HTB-81; RRID:CVCL_0105
Human: LNCaP (male)	ATCC	Cat#CRL-1740; RRID:CVCL_1379
Human: PC3 (male)	ATCC	Cat#CRL-1435; RRID:CVCL_0035
Experimental Models: Organisms/Strains		
Mouse: NOD-SCIDIL-2Rγ-/-Sex: male	Laboratory of Felsher	N/A
Mouse: KP53 Sex: male	AIPT colony (Laboratory of Malstrom)	N/A
Oligonucleotides		
See qPCR section for list of Primers used		
Software and Algorithms		
R	R Core Team. (2016). R: A Language and Environment for Statistical Computing (R Foundation for Statistical Computing) (Champely, 2018).	https://www.r-project.org/
GenePix Pro 6.0	Molecular Devices	http://mdc.custhelp.com/app/answers/detail/a_id/18691/~/genepix%C2%AE-pro-6-microarray-acquisition-%26-analysis-software-download-page
Image Lab 6.0	BioRad	http://www.bio-rad.com/en-us/product/image-lab-software?ID=KRE6P5E8Z
ImageStudioLite	LI-COR Biosciences	https://www.licor.com/bio/products/software/image_studio_lite/
ChemDraw Professional 15.0	PerkinElmer	http://www.perkinelmer.com/product/chemdraw-professional-chemdrawpro
GraphPad Prism 7	Prism	https://www.graphpad.com/scientific-software/prism/
SedFit	NIH	https://sedfitsedphat.nibib.nih.gov/software/default.aspx

(*Continued on next page*)

Continued

REAGENT or RESOURCE	SOURCE	IDENTIFIER
SedPhat	NIH	https://sedfitsedphat.nibib.nih.gov/software/default.aspx
AmiView V1.7.06	Spectral Instruments Imaging	https://specimg.com/instruments/ami/
BD FACSDIVA™ Software	BD Biosciences	http://www.bdbiosciences.com/us/instruments/research/software/flow-cytometry-acquisition/bd-facsdiva-software/m/111112/overview
Topsin 3.5 pl.7	Bruker	https://www.bruker.com/service/support-upgrades/software-downloads/nmr.html

CONTACT FOR REAGENT AND RESOURCE SHARING

Further information and requests for resources and reagents should be directed to and will be fulfilled by the Lead Contact, Angela N. Koehler (koehler@mit.edu).

EXPERIMENTAL MODEL AND SUBJECT DETAILS

Animal Studies

Mouse experiments were approved by the Institutional Animal Care and Use Committee (IUCAC) at the Massachusetts Institute of Technology or the Administrative Panel on Laboratory Animal Care (APLAC) at Stanford University, and were carried out in accordance with institutional and national guidelines. The efficacy studies used 4-6 week-old male NOD-SCIDIL-2Rγ-/- (NSG) mice. The cell lines used for transplantation experiments (4188 (T-ALL), and EC4 (HCC)) were isolated from tumors of male mice. The PK experiments used 6-9 month-old male LSL-Kras G12D/+ ; Trp53 flox/flox mice.

Cell Lines

Cell lines were obtained from ATCC with exception of P493-6, which was a gift from D. Eick. Cell lines were not authenticated in our hands. Cell lines were tested intermittently throughout studies using MycoAlert Mycoplasma Detection Kit (Lonza, Cat#LT07-418), generally a few days after thawing and immediately before significant studies (e.g. RNA-seq experiment). Cells were cultured in a humidified incubator at 37.0°C and 5.0% CO_2. P493-6 cells were cultured in RPMI Medium 1640 (gibco, 11875-093) supplemented with 10% Tet-approved FBS (Takara, Cat#631106) and penicillin-streptomycin (Corning, 30-002-CI). HEK293T (female) cells were cultured in Dulbecco's Modified Eagle Medium (DMEM) (gibco, Cat#11965-092) supplemented with penicillin-streptomycin and 10% FBS (ATCC, Cat#30-2020). PC12 cells were cultured in RPMI-1640 supplemented with penicillin-streptomycin, 5% FBS and 10% heat-inactivated horse serum. ST-486 (female), NCI-H1963 (male), NCI-H446 (male), NCI-H82 (male), SNU-398 (male), PSN-1 (male), COLO-320 DM (female), HCC-1599 (female), SNU-16 (female), MSTO-211H (male), LNCaP (male), PC3 (male) cells were cultured in RPMI-1640 supplemented with penicillin-streptomycin and 10% FBS. CA46 (male) and P3HR1 (male) cells were cultured in RPMI-1640 supplemented with penicillin-streptomycin and 20% FBS. HL-60 (female) cells were cultured in Iscove's Modified Dulbecco's Medium (IMDM) (ATCC, Cat#30-2005) supplemented with penicillin-streptomycin and 20% FBS. SKNMC (female), U87-MG (male), T98G (male), DU145 (male) cells were cultured in Eagle's Minimum Essential Medium (EMEM) (ATCC, Cat#30-2003) supplemented with penicillin-streptomycin and 10% FBS. NCI-H929 (female) cells were cultured in RPMI-1640 supplemented with penicillin-streptomycin, 0.05 mM 2-mercaptoethanol and 10% FBS.

METHOD DETAILS

Chemical Synthesis

KI-MS2-001, KI-MS2-002 and 2-(azidomethyl)benzaldehyde were prepared according to published procedures (Mitchell and Shaw, 2006). For the SMM screen, the compounds were originally synthesized as part of a diversity-oriented chemical library on solid phase involving 529 compounds involving a key catalytic enantioselective Suga-Ibata cycloaddition between an oxazole and aldehyde so as to develop enantiomerically pure compounds. Upon resynthesis, the compounds were prepared using a modified procedure carried out in solution that did not provide enantiomerically pure material. For **KI-MS2-001** and **KI-MS2-008**, the racemic mixtures (**KI-MS2-001**[a] and **KI-MS2-008**[a]) were separated into the respective enantiomers (**KI-MS2-001**[b-c] and **KI-MS2-008**[b-c], respectively) and tested in follow-up assays.

Synthesis of KI-MS2-008

KI-MS2-008 was obtained as a mixture of enantiomers according to the procedure outlined below.

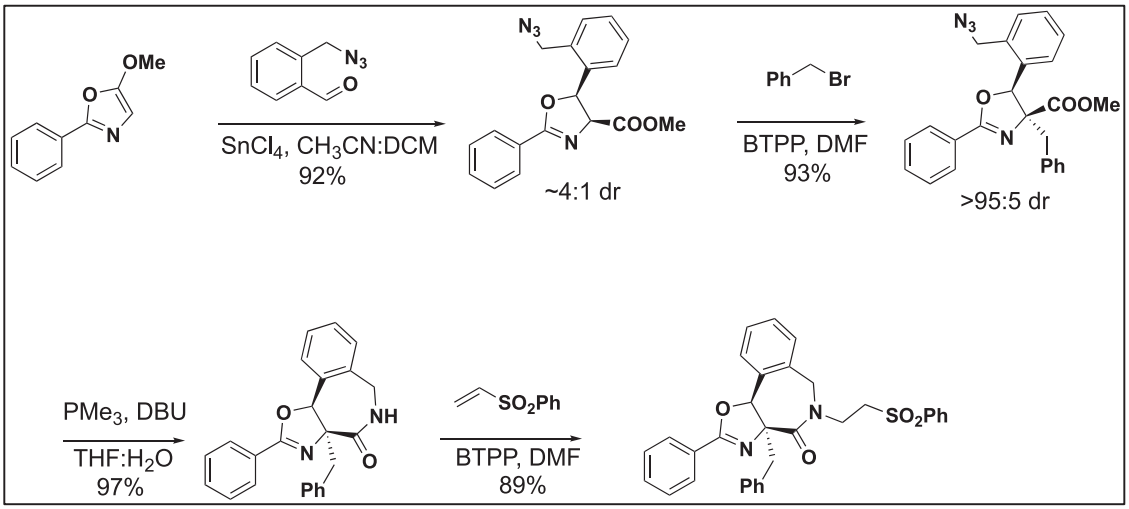

5-Methoxy-2-phenyloxazole was synthesized using the method reported by Mitchell et al. with minor modifications:

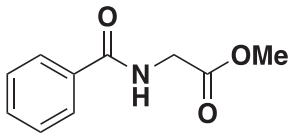

Methyl Benzoylglycinate

To a solution of benzoic acid (4.35 g, 35.31 mmol) and glycine methyl ester hydrochloride (4.03 g, 32.10 mmol) in DMF (50 mL) was added EDC hydrochloride (6.77 g, 35.31 mmol), HOBt (4.77 g, 35.31 mmol) and DIPEA (12.30 mL, 70.62 mmol) at room temperature. The mixture was stirred overnight, prior to being quenched with sat. $NaHCO_3$ (150 mL). The aqueous layer was extracted with EtOAc (3 x 30 mL), and the combined organic layers were washed with sat. $NaHCO_3$ (1 x 20 mL), brine (2 x 30 mL), dried over $MgSO_4$, filtered and concentrated to furnish **methyl benzoylglycinate** as an off-white solid (6.07 g, 98% yield). HRMS (m/z): $[M]^+$ calcd. for $C_{10}H_{11}NO_3$, 176.0706; found 176.0698.

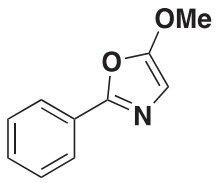

5-methoxy-2-phenyloxazole

A solution of **methyl benzoylglycinate** (4.25 g, 22.00 mmol) and Et_3N (14.7 mL, 104.5 mmol) in CH_2Cl_2 (10 mL) was added dropwise to a solution of iodine (12.56 g, 49.48 mmol) and triphenylphosphine (12.98 g, 49.48 mmol) in CH_2Cl_2 (150 mL) at room temperature. After 5 hr, the mixture was concentrated and purified by short plug on silica gel (15 to 40% EtOAc in hexanes) to provide **5-methoxy-2-phenyloxazole** (3.8 g, 98% yield). HRMS (m/z): $[M]^+$ calcd. for $C_{10}H_9NO_2$, 176.0706; found 176.0698.

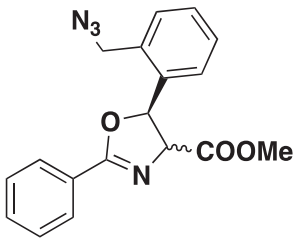

Methyl (5S)-5-(2-(azidomethyl)phenyl)-2-phenyl-4,5-dihydrooxazole-4-carboxylate (KI-MS2-082)

An oven-dried flask was charged with **5-methoxy-2-phenyloxazole** (2.54 g, 14.51 mmol), 2-(azidomethyl)benzaldehyde (2.58 g, 15.96 mmol) and anhydrous 1:1 CH_2Cl_2:CH_3CN (100 mL). The flask was purged with Arg, cooled to 0°C and $SnCl_4$ (17.6 mL, 1.0 M in CH_2Cl_2) was added. The reaction was stirred overnight at room temperature then cooled to 0°C. Saturated $NaHCO_3$ (100 mL) was carefully added followed by CH_2Cl_2 (75 mL) and the solution was vigorously stirred for 3 hr. The aqueous layer was extracted with EtOAc (4 x 30 mL). The combined organic layers were dried over $MgSO_4$, filtered concentrated and purified by column chromatography (10 to 45% EtOAc in hexanes) to afford **KI-MS2-082** (4.49 g, 92% yield) and as a mixture of diastereomers, as a yellow oil. KI-MS2-082cis (higher R_f) ^{1}H NMR (500 MHz, $CDCl_3$): δ 8.10 (d, *J* = 8.0 Hz, 2H), 7.55 (m, 1H), 7.45-7.50 (m, 3H), 7.31-7.39 (m, 3H), 6.18 (d, *J* = 10.5 Hz, 1H), 5.35 (d, *J* = 10.5 Hz, 1H), 4.45 (d, *J* = 13.5 Hz, 1H), 4.37 (d, *J* = 13.5 Hz, 1H), 3.18 (s, 3H). ^{13}C NMR (125 MHz, $CDCl_3$): δ 169.8, 167.0, 135.1, 132.7, 132.4, 129.7, 129.1, 129.0, 128.8, 127.0, 126.9, 79.9, 73.9, 53.1, 52.1. KI-MS2-082Trans (lower R_f) ^{1}H NMR (500 MHz, $CDCl_3$): δ 8.08 (d, *J* = 8.0 Hz. 1H), 7.55 (t, *J* = 8.0 Hz, 1H), 7.46 (t, *J* = 8.0 Hz, 2H), 7.34-7.40 (4H, m), 6.21 (d, *J* = 7.0 Hz, 1H), 4.79 (d, *J* = 7.0 Hz, 1H), 4.55 (d, *J* = 13.5 Hz, 1H), 4.46 (d, *J* = 13.5 Hz, 1H), 3.87 (s, 3H). ^{13}C NMR (125 MHz, $CDCl_3$): δ 171.6, 165.8, 138.6, 132.5, 132.4, 130.5, 129.8, 129.1, 129.0, 128.7, 126.9, 126.4, 80.0, 77.3, 53.2, 52.6. HRMS (m/z): $[M]^+$ calcd. for $C_{18}H_{16}N_4O_3$, 337.1295; found 337.1268.

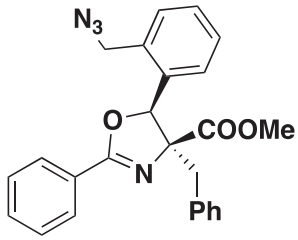

(±)-(4S,5S)-methyl 5-(2-(azidomethyl)phenyl)-4-benzyl-2-phenyl-4,5-dihydrooxazole-4-carboxylate (KI-MS2-006)

A cis/trans mixture of **KI-MS2-082** (4.49 g, 13.35 mmol) was diluted in DMF (50 mL). BTPP (5.40 mL, 17.35 mmol) was then added at room temperature followed by benzyl bromide (6.40 mL, 53.40 mmol), K_2CO_3 (3.69 g, 26.70 mmol) and TBAI (2.46 g, 6.67 mmol). After 16 hr, the reacting mixture was concentrated and purified by column chromatography on silica gel (5 to 40% EtOAc in hexanes) to afford **KI-MS2-006** (5.28 g, 93% yield) as a 95:5 dr. ^{1}H NMR (500 MHz, $CDCl_3$): δ 8.04 (m, 2H), 7.54 (m, 1H), 7.46 (m 2H), 7.39 (m, 2H), 7.23-7.38 (m, 7H), 5.93 (s, 1H), 4.58 (d, *J* = 14.0 Hz, 1H), 4.45 (d, *J* = 14.0 Hz, 1H), 3.57 (d, *J* = 13.5 Hz, 1H), 3.45 (d, *J* = 13.5 Hz, 1H), 3.16 (s, 3H). ^{13}C NMR (125 MHz, $CDCl_3$): δ 171.6, 165.0, 136.5, 135.2, 133.0, 132.2, 131.3, 130.0, 129.0, 128.8, 128.7, 128.4, 127.4, 127.2, 127.1, 84.7, 82.5, 53.0, 52.4, 45.0. HRMS (m/z): $[M]^+$ calcd. for $C_{25}H_{22}N_4O_3$, 427.1652; found 427.1678. The other diastereomer (lower R_f) can also be isolated. ^{1}H NMR (500 MHz, $CDCl_3$): δ 8.18 (d, *J* = 7.5 Hz, 2H), 7.62 (t, J = 7.5 Hz, 1H), 7.53 (t, *J* = 7.5 Hz, 2H), 7.46 (t, *J* = 7.5 Hz, 1H), 7.31-7.41 (m, 7H), 6.04 (s, 1H), 5.01 (d, *J* = 11.0 Hz, 1H), 4.74 (d, *J* = 14.5 Hz, 1H), 4.73 (d, *J* = 11.0 Hz, 1H), 3.15 (s, 3H).

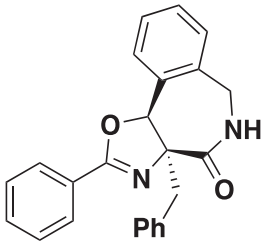

(±)-(3aS,10bS)-3a-benzyl-2-phenyl-5,6-dihydro-3aH-benzo[c]oxazolo[5,4-e]azepin-4(10bH)-one (KI-MS2-007)

KI-MS2-006 (1.73 g, 4.06 mmol) was diluted in THF:H_2O (10:1, 100 mL) followed by addition of DBU (0.64 mL, 4.26 mmol) and PMe_3 (4.50 mL, 1.0 M in THF) at room temperature. After 16 hr, water was added and the aqueous layer extracted with CH_2Cl_2 (x 3). The combined organic layers were dried over $MgSO_4$, filtered concentrated and purified by column chromatography on silica gel (0 to 15% MeOH in CH_2Cl_2) providing **KI-MS2-007** (1.21g, 81% yield). ^{1}H NMR (500 MHz, $CDCl_3$): δ 8.11 (d, *J* = 9.0 Hz, 2H), 7.56 (t, *J* = 7.5 Hz, 1H), 7.45 (t, *J* = 8.0 Hz, 2H), 7.36 (m, 2H), 7.16-7.32 (m, 7H), 5.84 (bs, 1H), 4.22 (m, 1H), 3.95 (dd, *J* = 15.5, 7.5 Hz, 2H), 3.51 (s, 2H). ^{13}C NMR (125 MHz, $CDCl_3$): δ 180.1, 165.9, 138.3, 134.3, 133.5, 131.3 (2), 129.5 (4), 128.8 (2), 128.5 (2), 128.4 (2), 128.2 (2), 127.5, 83.1, 65.0, 44.1, 32.3. HRMS (m/z): $[M]^+$ calcd. for $C_{24}H_{20}N_2O_2$, 369.1598; found 369.1580.

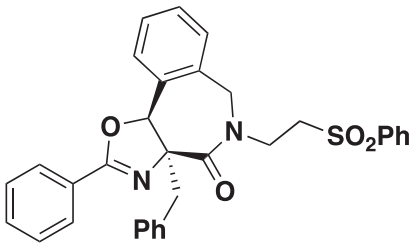

(±)- (3aS,10bS)-3a-benzyl-2-phenyl-5-(2-(phenylsulfonyl)ethyl)-5,6-dihydro-3aH-benzo[c]oxazolo[5,4-e]azepin-4(10bH)-one (KI-MS2-008)

To a solution of **KI-MS2-007** (1.10 g, 2.99 mmol) in DMF (15 mL) was successively added BTPP (1.20 mL, 3.86 mmol) and phenyl vinyl sulfone (1.00 g, 5.97 mmol) at room temperature. The reacting mixture was stirred overnight then diluted with water (50 mL). The aqueous layer was extracted with EtOAc (3 x 15 mL). The combined organic layers were dried over $MgSO_4$, filtered concentrated and purified by column chromatography (20 to 60% EtOAc in hexanes) to afford **KI-MS2-008** as a pale yellow solid (1.55 g, 97% yield). ^{1}H NMR (400 MHz, CD_3OD): δ 7.98 (dd, *J* = 14.5, 7.5 Hz, 3H), 7.94 – 7.84 (m, 1H), 7.74 (d, *J* = 7.0 Hz, 1H), 7.68 (t, *J* = 7.5 Hz, 2H), 7.58 (t, *J* = 7.5 Hz, 1H), 7.48 (t, *J* = 7.5 Hz, 2H), 7.41 – 7.36 (m, 1H), 7.36 – 7.26 (m, 3H), 7.24 – 7.15 (m, 2H), 5.93 (s, 1H), 4.57 (s, 1H), 4.44 – 4.24 (m, 1H), 3.92 (s, 1H), 3.71 (s, 1H), 3.56 – 3.39 (m, 2H). ^{13}C NMR (101 MHz, CD_3OD): δ 170.66, 146.59, 139.23, 136.87, 135.56, 134.38, 133.90, 133.86, 133.81, 133.57, 131.92, 130.90, 129.31, 129.29, 129.27, 128.31, 128.27, 128.16, 127.91, 127.85, 127.72, 127.69, 127.14, 126.85, 126.42, 125.71, 81.91, 74.25, 53.07, 49.97, 44.09, 43.11. HRMS (m/z): $[M]^+$ calcd. for $C_{32}H_{28}N_2O_4S$, 537.1845; found 537.1866.

Synthesis of KI-MS2-081 (Probe for Displaying Compound on Beads)

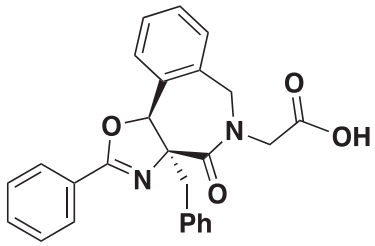

(±)-2-((3aS,10bS)-3a-benzyl-4-oxo-2-phenyl-3aH-benzo[c]oxazolo[5,4-e]azepin-5(4H,6H,10bH)-yl)acetic acid (KI-MS2-084)

To a solution of **KI-MS2-007** (300 mg, 0.81 mmol) in DMF (5 mL) were successively added BTPP (0.48 mL, 1.22 mmol) and *tert*-butyl bromoacetate (0.48 mL, 3.26 mmol). The resultant mixture was stirred overnight at room temperature and diluted with water (30 mL). The aqueous layer was then extracted with EtOAc (3 x 10 mL), and the combined organic layers were dried over $MgSO_4$, filtered concentrated and purified by column chromatography (5 to 60% EtOAc in hexanes) to afford (±)*tert*-butyl 2-((3aS,10bS)-3a-benzyl-4-oxo-2-phenyl-3aH-benzo[c]oxazolo[5,4-e]azepin-5(4H,6H,10bH)-yl)acetate (300 mg, 76% yield). The resulting ester was stirred overnight in 20% TFA/CH_2Cl_2 (15 mL). Upon completion, the mixture was concentrated azeotropically distilled with MeOH (x 3), and purified by column chromatography (0 to 15% MeOH in CH_2Cl_2) to afford **KI-MS2-084** as a white solid (210 mg, 0.49 mmol, 60% yield over 2 steps). ^{1}H NMR (400 MHz, CD_3OD): δ 7.94 (d, *J* = 7.5 Hz, 2H), 7.45 (t, *J* = 7.5 Hz, 2H), 7.34 (t, *J* = 7.5 Hz, 2H), 7.24 – 7.18 (m, 2H), 7.18 – 7.04 (m, 6H), 5.73 (s, 1H), 4.44 – 4.15 (m, 2H), 4.11 (q, *J* = 7.0 Hz, 1H), 3.98 – 3.56 (m, 1H), 3.52 – 3.23 (m, 2H). ^{13}C NMR (125 MHz, $CDCl_3$): δ 172.90, 171.64, 170.99, 132.44, 131.56 (2), 130.21, 129.02 (3), 128.85 (5), 128.62, 128.56 (2), 127.52, 127.44, 126.77, 71.97, 60.83, 50.94, 45.16, 30.09. HRMS (m/z): $[M]^+$ calcd. for $C_{26}H_{22}N_2O_4$, 427.1652; found 427.1678.

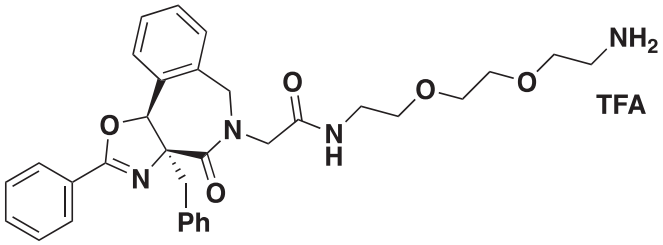

(±)-N-(2-(2-(2-aminoethoxy)ethoxy)ethyl)-2-((3aS,10bS)-3a-benzyl-4-oxo-2-phenyl-3aH-benzo[c]oxazolo[5,4-e]azepin-5(4H,6H,10bH)-yl)acetamide 2,2,2-trifluoroacetate (KI-MS2-081)

To a solution of **KI-MS2-084** (20 mg, 47 μmol) and *tert*-butyl (2-(2-(2-aminoethoxy)ethoxy)ethyl)carbamate (14 mg, 56 μmol) in DMF (1 mL) was added HATU (23 mg, 61 μmol) and DIPEA (17 μL, 94 μmol). The mixture was stirred for 18 hr, at room temperature after which time the mixture was concentrated and purified by column chromatography on silica gel (25 to 80% Acetone/hexanes) to afford the boc-protected product. The material was re-dissolved in 10% TFA/DCM, and stirred at room temperature for 5 hr, after which time the mixture was concentrated azeotropically distilled with MeOH (3 x), and purified by column chromatography (0 to 15% MeOH in CH_2Cl_2) to afford **KI-MS2-081** as a colorless oil (20 mg, 36 μmol, 77% yield over 2 steps). ^{1}H NMR (400 MHz, CD_3OD): δ 7.98 (d, *J* = 7.5 Hz, 2H), 7.60 (t, *J* = 7.5 Hz, 1H), 7.51 (t, *J* = 7.5 Hz, 2H), 7.44 (d, *J* = 7.5 Hz, 1H), 7.41 – 7.27 (m, 5H), 7.26 – 7.19 (m, 3H), 6.04 (s, 1H), 4.76 (bs, 1H), 4.32 (bs, 1H), 4.23 – 4.01 (m, 2H), 3.66 (s, 2H), 3.62 (t, *J* = 5.0 Hz, 2H), 3.59 – 3.55 (m, 2H), 3.55 – 3.47 (m, 4H), 3.41 – 3.35 (m, 2H), 3.21 (q, *J* = 7.4 Hz, 1H), 3.07 (t, *J* = 5.0 Hz, 2H), 1.31 (dd, *J* = 14.0, 6.5 Hz, 2H). ^{13}C NMR (125 MHz, CD_3OD): δ 171.49, 169.71, 148.64, 136.59, 134.41, 132.21, 130.98 (2), 128.50 (2), 128.40, 128.23 (4), 127.87 (3), 127.66, 127.02, 126.49, 87.94, 70.01, 69.95, 68.97, 66.80, 66.47, 51.91, 50.43, 44.59, 39.41, 38.89. HRMS (m/z): $[M]^+$ calcd. for $C_{32}H_{36}N_4O_5$, 557.2758; found 557.2757.

Synthesis of KI-MS2-085 (Diazirine/Alkyne Functionalized Probe)

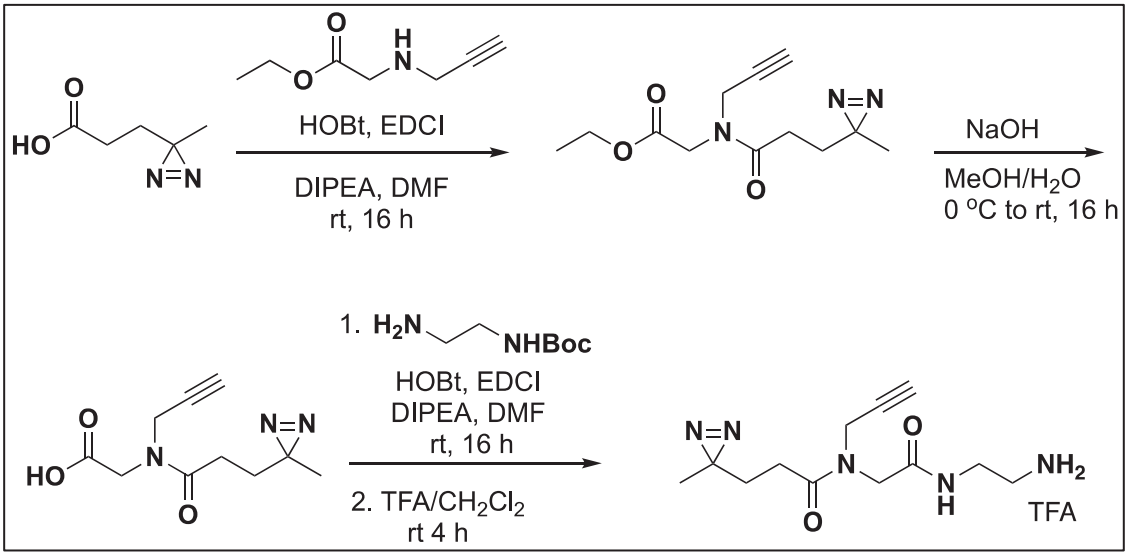

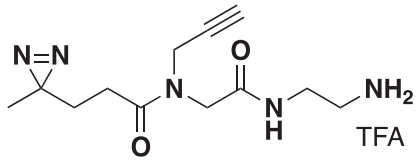

Preparation of N-(2-((2-aminoethyl)amino)-2-oxoethyl)-3-(3-methyl-3H-diazirin-3-yl)-N-(prop-2-yn-1-yl)propanamide 2,2,2-trifluoroacetate

To a solution of 3-(3-methyl-3H-diazirin-3-yl)propanoic acid (0.87 g, 6.70 mmol, prepared following Org. Lett. 15(19), 5060-5063, 2013) and ethyl 2-(prop-2-yn-1-ylamino)acetate (0.80 g, 5.66 mmol, prepared following Synthesis 3, 488-494, 2009) in DMF (10 mL) were added PyBop (2.95 g, 5.66 mmol) and DIPEA (1.97 mL, 11.32 mol). The mixture was stirred at room temperature for 18 hr, concentrated and purified by column chromatography on silica gel (25% EtOAc in hexanes) affording ethyl 2-(3-(3-methyl-3H-diazirin-3-yl)-N-(prop-2-yn-1-yl)propanamido)acetate (1.1 g). NaOH (0.39 g, 9.74 mmol) was added to the resulting ester (1.10 g, 4.87 mmol) in MeOH:H_2O (5:1, 20 mL) and the mixture was stirred overnight. The solvent was removed under vacuum, and the residue partitioned between CH_2Cl_2 and H_2O. 6N HCl was slowly added until pH 2 was reached and the product was extracted with CH_2Cl_2. The combined organic layers were dried over $MgSO_4$, filtered and concentrated affording the carboxylic acid (2-(3-(3-methyl-3H-diazirin-3-yl)-N-(prop-2-yn-1-yl)propanamido)acetic acid). LCMS: M+1=224. To a solution of the carboxylic acid (210 mg, 941 μmol) and *tert*-butyl (2-aminoethyl)carbamate (137 mg, 855 μmol) in DMF (2 mL) were added EDC hydrochloride (0.21 g, 1.11 mmol), HOBt (0.14 g, 1.03 mmol) and DIPEA (0.30 mL, 1.71 mmol). The reacting mixture was stirred at room temperature overnight, then diluted with sat. $NaHCO_3$, and the aqueous layer extracted with EtOAc. The combined organic layers were dried over $MgSO_4$, filtered and concentrated to afford the boc-protected product (*tert*-butyl

(2-(2-(3-(3-methyl-3H-diazirin-3-yl)-N-(prop-2-yn-1-yl)propanamido)acetamido)ethyl)carbamate) in good purity. This material was stirred in 10% TFA/DCM for 3 hr which showed completed conversion by LCMS. The mixture was concentrated and azeotropically distilled with MeOH (3x) to afford N-(2-((2-aminoethyl)amino)-2-oxoethyl)-3-(3-methyl-3H-diazirin-3-yl)-N-(prop-2-yn-1-yl)propanamide 2,2,2-trifluoroacetate.

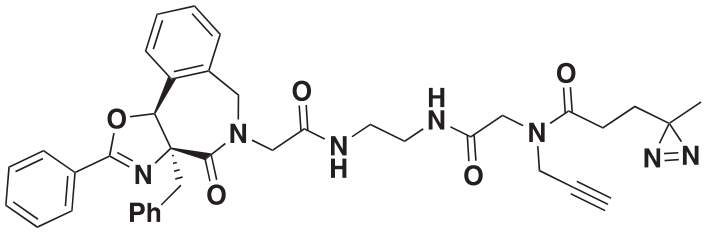

(±)-N-(2-((2-(2-((3aS,10bS)-3a-benzyl-4-oxo-2-phenyl-3aH-benzo[c]oxazolo[5,4-e]azepin-5(4H,6H,10bH)-yl) acetamido)ethyl)amino)-2-oxoethyl)-3-(3-methyl-3H-diazirin-3-yl)-N-(prop-2-yn-1-yl)propanamide (KI-MS2-085)

To a solution of **KI-MS2-084** (3 mg, 7.0 μmol) and N-(2-((2-aminoethyl)amino)-2-oxoethyl)-3-(3-methyl-3H-diazirin-3-yl)-N-(prop-2-yn-1-yl)propanamide 2,2,2-trifluoroacetate (3 mg, 8.5 μmol) in DMF (0.3 mL) were added HATU (4 mg, 9.1 μmol) and DIPEA (4 μL, 21 μmol). The mixture was stirred for 18 hr, concentrated and purified by preparative TLC (7% MeOH in CH_2Cl_2) to afford **KI-MS2-085** (4 mg, 5.9 μmol, 85% yield over 2 steps). ^{1}H NMR (400 MHz, $CDCl_3$): δ 8.03 (d, *J* = 7.5 Hz, 2H), 7.59 (t, *J* = 7.5 Hz, 1H), 7.47 (t, *J* = 7.5 Hz, 2H), 7.35 (m, 6H), 7.27 (m, 4H), 6.90 (s, 1H), 5.87 (s, 1H), 4.24 (m, 2H), 4.07 (s, 2H), 3.87 (m, 1H), 3.51 (m, 2H), 3.26 (m, 3H), 2.36 (m, 2H), 1.74 (m, 2H), 1.43 (d, *J* = 6.5 Hz, 1H), 1.00 (s, 3H). ^{13}C NMR (125 MHz, $CDCl_3$): δ 172.55, 171.93, 170.50, 170.02, 169.76, 169.17, 168.45, 167.93, 134.42, 133.08, 131.25, 128.98, 128.94, 128.85, 128.55, 128.47, 127.58, 125.37, 78.66, 77.79, 73.58, 72.93, 54.16, 53.41, 51.01, 50.15, 49.79, 44.88, 40.09, 40.00, 38.98, 38.79, 36.11, 29.45, 29.37, 27.34, 27.27, 25.55. HRMS (m/z): $[M]^+$ calcd. for $C_{38}H_{39}N_7O_5$, 674.3085; found 674.3070.

Small Molecule Microarray

Small molecule microarrays were manufactured and analyzed against purified Max as previously described (Clemons et al., 2010) Briefly, pure His6-tagged Max (Panomics, Cat # RP0080) was incubated on glass slides with printed compounds at 1 μg/mL in TBST buffer supplemented with 5 mM $MgCl_2$ and 10% (v/v) glycerol. Binding to the arrays was detected using an Alexa Fluor® 647-conjugated monoclonal anti-His5 antibody (Qiagen, Cat #35370) at 1:1000 dilution in the same buffer. Incubated arrays were scanned using an Axon 4000B scanner at 5 μm resolution using 635 nm and 532 nm lasers to detect assay positives and printed sentinels. Screened arrays were analyzed using GenePix Pro 6.0 software from Molecular Devices and hit calls were determined as outlined in the Clemons et al. manuscript.

Transcriptional Reporter Assay

HEK 293T cells were transfected with the Myc reporter construct (Devgan et al., 2012) (Cignal Myc Reporter (luc) Kit; #CCS-012L, Qiagen) by adding attractene and Myc reporter to cells in OptiMEM. Specifically, 0.6 μL of attractene and 25 μL of OptiMEM were mixed per well, in addition to 0.5 μL of Myc reporter and 25 μL of OptiMEM. After 5 min, these two solutions were mixed together and incubated at room temperature for 30 min. 20,000 cells in OptiMEM with 5% (v/v) FBS and no antibiotics were seeded into each well and 50 μL of the attractene/Myc reporter solution was added to each well. Cells were allowed to incubate at 37°C for about 17 hr. Media was aspirated and replaced with 50 μL OptiMEM + 0.5% (v/v) FBS with 1x nonessential amino acids for each well. ~7 hr later, media was aspirated and replaced with 50 μL of media containing 0.4% (v/v) DMSO and compound concentrations ranging from 0 to 40 μM. After 16 hr of compound treatment, cells were allowed to reach room temperature. 50 μL of Dual-Glo Luciferase Reagent (#E2940, Promega) was added to each well and plates were incubated for 15 min, followed by a luminescence reading for firefly luciferase activity (automatic attenuation, 500 ms integration time). 50 μL of Dual-Glo Stop & Glo Reagent (Promega) was added to each well and incubated for 15 min, followed by another luminescence reading for *Renilla* luciferase activity.

Viable Cell Assay

96-well plates were seeded with 2000 or 5000 cells in 100 μL media with 0.4% (v/v) DMSO and compound concentrations ranging from 0 to 40 μM. For some conditions, 0.1 μg/ mL doxycycline (D9891, Sigma) and/or 1 μM β-estradiol (E2758, Sigma) was added to the cell culture. After the appropriate amount of time (3 – 5 days), plates were allowed to reach room temperature for 30 min and 100 μL of CellTiter-Glo reagent (#G7572, Promega) was added to each well. The plates were placed on a shaker with medium setting for 2 min and allowed to incubate at room temperature for 10 min. Plates were read for luminescence with automatic attenuation and 500 ms integration time.

Flow Cytometry

P493-6 cells were treated with 0 – 40 μM **KI-MS2-008** for 3 – 5 days. 1 – 5 million cells were resuspended in PBS with or without 10 μg/mL propdium iodide (81845, Sigma-Aldrich). Cell mixtures were passed through a cell strainer (352235, Falcon), and counted using a BD FACSCANTO™ II (BD BioSciences), and analyzed with BD FACSDIVA™ software.

Bead-Based Lysate Pull-down with KI-MS2-081

50 μL of well-mixed NHS activated magnetic beads (#88826, ThermoFisher Scientific) were washed in DMSO three times. 100 μL of DMSO, 0.5 μL of 10 mM KI-MS2-081 or DMSO and 0.75 μL of triethylamine were added to the beads. The mixture was protected from light and allowed to rotate overnight at room temperature. The next day, aminoethanol (2.5 μL) was added to the mixture and allowed to incubate at room temperature overnight. The third day, beads were washed once in DMSO, followed by three washes in wash buffer (150 mM NaCl, 50 mM Tris, protease inhibitor cocktail, phosphatase inhibitor cocktail, pH 7.5). Whole cell lysate was prepared by washing P493-6 cells in cold PBS twice and resuspending in lysis buffer (200 mM NaCl, 50 mM Tris, 1% (w/v) NP-40, 0.1 g/100 mL sodium deoxycholate, protease inhibitor cocktail, phosphatase inhibitor, 0.4 μL benzonase/10 mL buffer) at a density of roughly 50 million cells/mL. Following a brief vortex, this mixture was iced for 20 min and centrifuged at 4°C for 10 min at 14,000 g. 4 mg of protein was incubated with the washed beads for 1 hr. The beads were washed three times in wash buffer and boiled in 50 μL 2x SDS loading buffer (#1610737, Bio-Rad) at 90°C for 5 min. c-Myc and Max proteins were visualized on immunoblots using anti-c-Myc antibody (9E10, Santa Cruz Biotechnology) and anti-Max antibody (C-124, Santa Cruz Biotechnology), with anti-mouse IgG, HRP-linked Antibody (#7076, Cell Signaling Technology) and anti-rabbit IgG, HRP-linked antibody (#7074, Cell Signaling Technology) as secondary antibodies.

In Vitro Labeling of Max with KI-MS2-085

In the case of non-covalent probes, photoaffinity tags can be added to create a covalent bond between the probe and protein target in addition to a clickable handle to ensure pull-down of all targets including the lower affinity binders. (Blencowe and Hayes, 2005; Mackinnon and Taunton, 2009; Smith and Collins, 2015) The alkyne handles can be clicked to a fluorophore to visually analyze the protein targets. (Speers and Cravatt, 2009).

Recombinant human Max protein (1 μL, 50 μg/μL, Abcam, ab95309) was treated with DMSO or 5 μM **KI-MS2-085**. After treating for 1 hr, the samples were irradiated at 365 nm for 10 min (except for the –UV sample). The proteins were incubated with AlexaFluor™ 647 azide (1 μL, 10 mM, ThermoFisher Scientific, #A10277), TCEP (1 μL, 50 mM), and TBTA (3 μL, 1.7 mM). After a brief vortex, $CuSO_4$ (1 μL, 50 mM) was added and the click reaction was incubated at room temp for 1 hr. The **KI-MS2-085**-labeled samples were added to loading buffer (25 μL, 2X Laemmli Sample Buffer, Bio-Rad, #1610737) and the proteins were boiled at 90°C for 5 min. Each sample was loaded onto a 4-20% denaturing PAGE gel. Samples were electrophoresed at 200V until the loading dye was at the bottom of the gel. The gels were visualized using the Odyssey classic infrared imaging system (LI-COR Biotech.). After visualization, **KI-MS2-085**-labeled Max was submitted for MALDI analysis.

Live-Cell Pull-down with KI-MS2-085

P493-6 cell culture (5 mL) at 1-2 million cells/mL was treated with DMSO, 2.5, 5, or 10 μM **KI-MS2-085**, or 10 μM **KI-MS2-085** with 40 μM **KI-MS2-008**. After treating for 1 hr, the cells were washed in PBS at 4°C and irradiated at 365 nm for 10 min (except for the –UV sample). The cells were pelleted and resuspended in lysis buffer (200 mM NaCl, 50 mM Tris, 1% (w/v) NP-40, 0.1 g/100 mL sodium deoxycholate, protease inhibitor cocktail) and incubated on ice for 25 min. The supernatant was recovered by spinning at 14000 g for 10 min at 4°C. The **KI-MS2-085**-labeled lysates were diluted with H_2O (400 μL) and incubated with Albumin depletion resin (200 μL slurry, ThermoFisher Scientific, #85160) for 10 min at room temp. The beads were filtered at 14000 g for 1 min. The beads were washed once with PBS (100 μL) and filtered at 14000 g for 1 min.

The lysates (500 μL) were incubated with AlexaFluor™ 647 azide (1 μL, 10 mM, ThermoFisher Scientific, #A10277), TCEP (1 μL, 50 mM), and TBTA (3 μL, 1.7 mM). After a brief vortex, $CuSO_4$ (1 μL, 50 mM) was added and the click reaction was incubated at room temp for 1 hr.

Acetone (600 μL, chilled to -20°C) was added to the HSA-free lysates. The precipates were pelleted at 21,000 g for 6 min. The pellet was dispersed in acetone (1000 μL, chilled to -20°C) using a sonicator. These steps were repeated twice. The resulting pelleted lysates were resuspended in 1% (w/v) SDS in PBS (100 μL). The protein was quantified by Bradford assay. Protein lysates (50 μg) was added to loading buffer (25 μL, 2X Laemmli Sample Buffer, Bio-Rad, #1610737) and the proteins were boiled at 90°C for 5 min. Each sample was loaded onto a 4-20% denaturing PAGE gel. Samples were electrophoresed at 200V until the loading dye was at the bottom of the gel. The gels were visualized using the Odyssey classic infrared imaging system (LI-COR Biotech.). Relative Max protein levels were determined via immunoblotting, using anti-Max antibody (ab199489, Abcam) and IRDye® 800CW Goat anti-Rabbit IgG (925-32211, LICOR).

Electrophoretic Mobility Shift Assay

For c-Myc/Max heterodimer disruption: Binding reactions containing binding buffer (2 μL of a 10X solution; 10X solution: 10X PBS, 1 mM EDTA, 1% (w/v) NP-40, 50% (v/v) glycerol), P493-6 lysate (0.5 μg, prepared fresh), **KI-MS2-008** (or DMSO, 10058-F4), and

DNase/RNase free H_2O (to a final volume of 20 μL) were prepared in microcentrifuge tubes (0.65 mL) and incubated at 37°C for 20 min. AlexaFluor™ 660-labeled E-Box DNA (1 μL, 50 fmol/μL, IDT) was added to the binding reaction and then incubated at 37°C for 10 min.

For Max/Max homodimer induction: Binding reactions containing binding buffer (2 μL of a 10X solution; 10X solution: 10X PBS, 1 mM EDTA, 1% (w/v) NP-40, 50% (v/v) glycerol), KCl (6 μL, 1 M), recombinant Max (1 μL, 12.5 ng/μL, Abcam, ab95309), **KI-MS2-008** (or DMSO, NSC13728), and DNase/RNase free H_2O (to a final volume of 20 μL) were prepared in microcentrifuge tubes (0.65 mL) and incubated at room temp for 20 min. AlexaFluor™ 660-labeled E-Box DNA (1 μL, 50 fmol/μL, IDT) was added to the binding reaction and then incubated at room temp for 10 min.

Loading dye (1 μL, 20X solution; 0.5X TBE, 40% (v/v) glycerol, 2 mg/mL Orange G dye, Sigma) was added to each reaction and samples were loaded onto a 4-20% non-denaturing PAGE gel that was pre-run at 200 V for 1 hr in 0.5X TBE. Samples were electrophoresed at 200V until the loading dye was ~$^3/_4$ down the gel. The gels were visualized using the Odyssey classic infrared imaging system (LI-COR Biotech.).

Analytical Ultracentrifugation

Recombinant human Max protein (Abcam, ab95309) was dialyzed (50 mM phosphate, pH 7.2, 100 mM NaCl, 1 mM EDTA) three times to stabilize the chemical potential of the protein. Three samples were prepared for the experiment. Max protein (450 μL, 0.056 mg/ml) with DMSO and Max protein (450 μL, 0.056 mg/ml) pre-incubated (30 min) with **KI-MS2-008** (10 μM or 20 μM) were added to the analytical ultracentrifugation (AUC) assembly cells. The assembly cells were positioned into a Beckman XL-I Analytical Ultracentrifuge and centrifuged at 42,000 rpm at 20°C. Sedimentation velocity experiments were started scanning A_{280} every ~1.2 min for 18 hr. The data (both absorbance and interference) were analyzed with SedFit software utilizing the continuous c(s) distribution model keeping resolution (200), partial specific volume (0.707), buffer density (1.00), buffer viscosity (0.01002), bottom (7.15), and one sigma confidence level (0.68) constant. The data were fitted for the frictional ratio (1.68 for DMSO, 1.22 for 10 μM, and 1.53 for 20 μM), meniscus (5.94 for DMSO and 10 μM, and 5.92 for 20 μM), baseline (0.00 for all samples), RI noise, and time independent noise. The estimations for the molecular weights of the two species were 25 kDa and 51 kDa, respectively.

The data were exported from SedFit and imported into SedPhat. The data were analyzed in SedPhat utilizing the monomer-dimer self-association model (Brautigam, 2011) keeping M1 (20,000), S1 (1.964 for DMSO, 1.770 for 10 μM, and 1.964 for 20 μM), S2 (2.683 for DMSO, 2.447 for 10 μM, and 2.685 for 20 μM), mass conservation, and $\log_{10}$ nonid sed field (-2.0458) constant. The data were fitted for logKa (5.12153 for DMSO, 7.93937 for 10 μM, and 8.01024 for 20 μM), logk- (-1.02487 for DMSO, -1.21487 for 10 μM, and -1.01234 for 20 μM), and incompetent fraction (0.00000 for DMSO, 0.03591 for 10 μM, and 0.04173 for 20 μM).

Size Exclusion Chromatography

Recombinant human Max protein (Abcam, ab95309) was dialyzed (50 mM phosphate, pH 7.2, 100 mM NaCl, 1 mM EDTA) three times to stabilize the chemical potential of the protein. Two samples were prepared for the experiment. Max protein (429 μL, 0.50 mg/mL and 0.056 mg/ml) with DMSO and Max protein (429 μL, 0.50 mg/mL and 0.056 mg/ml) pre-incubated (30 min) with **KI-MS2-008** (10 μM) were injected onto a Superdex 200 GL size exclusion column using 100% buffer (50 mM $NaHPO_4$, 150 mM NaCl, 1 mM BME, 5% (v/v) glycerol, and 2% (v/v) DMSO) to separate the species in solution. The monomer vs. dimer distribution was analyzed by integrating the A_{280}.

Cellular Thermal Shift Assay (Molina et al., 2013)

Protocol adapted from Jafari et al. (Jafari et al., 2014). For dose dependent CETSA, DMSO or **KI-MS2-008** (0.078 μM, 0.156 μM, 0.313 μM, 0.625 μM, 1.25 μM, 2.50 μM, and 5.00 μM) were incubated with 4 x 10^6 cells for 1 hr at 37°C. For time course CETSA, 10 μM **KI-MS2-008** was incubated with 4 x 10^6 cells for 0, 0.25 hr, 0.5 hr, 0.75 hr, 1 hr, 4 hr, 8 hr, and 24 hr at 37°C. Cells were then washed and harvested with cold PBS. After transferring to falcon tubes these were spun down for 3 min at 500 g, and the supernatant discarded. The cell pellet was resuspended in PBS containing protease inhibitor cocktail (100 μL) and transferred to PCR tubes. Cells were heat shocked in a thermal cycler at 60.0°C for 3 min. The cell suspensions were then subjected to three freeze-thaw cycles with liquid nitrogen to lyse cells. For a uniform thawing this step was performed in a thermal cycler at 25°C. Lysates were spun at 21,000 g for 45 min at 4°C to clarify and pellet aggregated protein. The tubes were carefully handled after this step to avoid disturbing the pellet. The supernatant containing the soluble protein fraction was transferred to a new tube. Protein lysates (7.5 μL) was added to loading buffer (7.5 μL, 2X Laemmli Sample Buffer, Bio-Rad, #1610737) and the proteins were boiled at 90°C for 5 min. Each sample was loaded onto a 4-20% denaturing PAGE gel. Samples were electrophoresed at 200 V until the loading dye was at the bottom of the gel. Relative c-Myc and Max protein levels were determined via immunoblotting, using anti-c-Myc antibody (9E10, Santa Cruz Biotechnology) and anti-Max antibody (ab199489, Abcam).

^{15}N-Heteronuclear Single Quantum Coherence

Experiments were conducted at NMX. HSQC was performed on 15^N-Max*VL(tr) (50 μM in 50 mM NaPi pH 6.8, 250 mM KCl, 3.6% DMSO d-6 and 10% D_2O at 35°C) in the absence and presence of **KI-MS2-008** (150 μM). Protein NMR was recorded on a Bruker Avance600 with the HSQCETFPF3GPSI sequence: 2D [^{1}H,^{15}N]-correlation *via* double inept transfer using sensitivity improvement; ^{15}N-decoupling during acquisition using the F3 channel; phase sensitive using Echo/Antiecho-TPPI gradient selection; and a flip-back water pulse (Grzesiek and Bax, 1993; Kay et al., 1992; Palmer et al., 1991; Schleucher et al., 1994).

Time Course of Protein Levels

P493-6 cell culture (5 mL) at 1-2 million cells/mL was treated with 10 μM **KI-MS2-008** or 0.1% (v/v) DMSO. After the indicated time, cells were washed in PBS at 4°C, resuspended in lysis buffer (200 mM NaCl, 50 mM Tris, 1% (w/v) NP-40, 0.1 g/100 mL sodium deoxycholate, protease inhibitor cocktail, phosphatase inhibitor, 0.4 μL benzonase/10 mL buffer) and incubated on ice for 20 min. The supernatant was recovered by spinning at 14,000 g for 10 min at 4°C. Relative protein levels were determined via immunoblotting, using anti-c-Myc antibody (9E10, Santa Cruz Biotechnology), anti-c-Myc (pT58) antibody (ab28842, Abcam), anti-c-Myc (pS62) antibody (ab78318), anti-Max antibody (ab199489, Abcam), anti-MLX antibody (sc393086, Santa Cruz Biotechnology), anti-Mxd1 antibody (sc8012, Santa Cruz Biotechnology), anti-Mxd4 antibody (sc1221, Santa Cruz Biotechnology) and anti-vinculin antibody (V 9131, Sigma).

RNA-seq

Cells were plated in 6-well plates at a concentration of 3 million cells in 3 mL media and treated with 1 μM or 10 μM **KI-MS2-008**, 0.1 μg/mL doxycycline, or DMSO for 8 hr with 4 replicates per condition. RNA was isolated from each sample guided by the Aurum™ Total RNA Mini Kit (Bio-Rad). RNA samples were quantified and quality assessed using an Advanced Analytical Fragment Analyzer. 20 ng of total RNA was used for library preparation with ERCC Spike-in control Mix A (Ambion 10^{-6} final dilution). All steps were performed on a Tecan EVO150. 3'DGE-custom primers 3V6NEXT-bmc#1-24 were added to a final concentration of 1.2 μM. (5'-/5Biosg/ACACTCTTTCCCTACACGACGCTCTTCCGATCT[BC_6]$N_{10}T_{30}$VN-3' where 5Biosg = 5' biotin, [BC6] = 6bp barcode specific to each sample/well, N10 = Unique Molecular Identifiers, Integrated DNA technologies).

After addition of the oligonucleotides, samples were denatured at 72°C for 2 min followed by addition of SMARTScribe RT per manufacturer's recommendations with Template-Switching oligo5V6NEXT (12μM, [5V6NEXT : 5'-iCiGiCACACTCTTTCCCTACACGA CGCrGrGrG-3' where iC: iso-dC, iG: iso-dG, rG: RNA G]) and incubation at 42°C for 90 min followed by inactivation at 72°C for 10 min. Following the template switching reaction, cDNA from 24 wells containing unique well identifiers were pooled together and cleaned using RNA Ampure beads at 1.0X. cDNA was eluted with 90 μL of water followed by digestion with Exonuclease I at 37°C for 45 min, inactivation at 80°C for 20 min. Single stranded cDNA was then cleaned using RNA Ampure beads at 1.0X and eluted in 50 μL of water.

Second strand synthesis and PCR amplification was done using the Advantage 2 Polymerase Mix (Clontech) and the SINGV6 primer (10 pmol, Integrated DNA Technologies 5'-/5Biosg/ACACTCTTTCCCTACACGACGC-3'). 12 cycles of PCR were performed followed by clean up using regular SPRI beads at 1.0X, and was eluted with 20 μL of EB. Successful amplification of cDNA was confirmed using the Fragment Analyzer. Illumina libraries were then produced using standard Nextera tagmentation substituting P5NEXTPT5-bmc primer (25μM, Integrated DNA Technologies, (5'-AATGATACGGCGACCACCGAGATCTACACTCTTTCCCTACA CGACGCTCTTCCG*A*T*C*T*-3' where * = phosphorothioate bonds.) in place of the normal N500 primer. Final libraries were cleaned using SPRI beads at 0.8X and quantified using the Fragment Analyzer and qPCR before being loaded for paired-end sequencing using the Illumina NextSeq500. Post-sequencing, quality-control on each of the libraries was performed to assess coverage depth, enrichment for messenger RNA (exon/intron and exon/intergenic density ratios), fraction of rRNA reads and number of detected genes using bespoke scripts. Sequences were aligned against the human genome hg19 and ERCC reference sequences separately using bwa [http://bio-bwa.sourceforge.net/]. Gene expression was estimated based on reads mapping near the 3' end of transcripts using ESAT (Derr et al., 2016) based on the hg19 Refseq annotation. Results were summarized as counts per million mapped reads (CPMs), merged across samples, log-transformed and subjected to hierarchical clustering and visualization. For ERCC quantification, bam files from bwa were sorted and indexed with samtools (Li et al., 2009) and counts were retrieved from the indices using idxstats (Anders and Huber, 2010; Benjamini and Hochberg, 1995; Cook, 1977; Langmead et al., 2009; Li et al., 2009; Love et al., 2014; Soumillon et al., 2014).

qPCR

Cells were plated in 6-well plates at a concentration of 3 million cells/mL in 3 mL media and treated with 10 μM **KI-MS2-008**, 10 μM MG132, both **KI-MS2-008** and MG132, or 0.4% (v/v) DMSO for 15 min, 30 min, 45 min, 1 hr , 2 hr or 4 hr. RNA was isolated from each sample guided by the Aurum™ Total RNA Mini Kit (Bio-Rad). RNA samples were quantified using a NanoDrop One^C (Thermo Scientific). A High Capacity cDNA Reverse Transcription Kit (appliedbiosystems) was used to generate cDNA from the isolated RNA. Primers (Eurofins) and PowerUp™ SYBR™ Green Master Mix (appliedbiosystems) were added to cDNA samples and DNA was amplified using a CFX384 Touch™ Real-Time PCR Detection System (Bio-Rad). Data was normalized to DMSO controls and beta-actin for a reference gene, using the ΔΔCt method (Livak and Schmittgen, 2001).

Primers for qPCR

APEX1: forward primer – 5'-CAGATCTCGCGAGTAGGGCAACG-3';
reverse primer – 5'-GTCTTACTCTTCTTGGCCTCTGG-3'.
DUSP2: forward primer – 5'-GGGCTCCTGTCTACGACCA-3';
reverse primer – 5'-GCAGGTCTGACGAGTGACTG-3'.
HK2: forward primer – 5'-GGGACAATGGATGCCTAGATG-3';
reverse primer – 5'-GTTACGGACAATCTCACCCAG-3'.
IPO4: forward primer – 5'-CTCGCAAGTTGTACGCAATGC-3';

reverse primer – 5'-GGCACCGACTTCAAGTAGGC-3'.
MAX: forward primer – 5'-ATAATGCACTGGAACGAAAACG-3';
reverse primer – 5'-TGGCTTTGTCTAGGATTTGGG-3'.
MYC (Lu et al., 2010): forward primer – 5'-AAACACAAACTTGAACAGCTAC-3';
reverse primer – 5'-ATTTGAGGCAGTTTACATTATGG-3'.
PES1: forward primer – 5'-GGGCATTTATCCCCATGAACC-3';
reverse primer – 5'-CACCTTGTATTCACGGAACTTGT-3'.
PPRC1: forward primer – 5'-AAGACAGCTCTGCAGAGAAGC-3';
reverse primer – 5'-CCACAGGTTTGCTTACAGGTG-3'.
RRP12: forward primer – 5'-GTGACCTGACAGTCGATGCTG-3';
reverse primer – 5'-AAAGGCCACTCAGGAAGGTAC-3'.
SRM: forward primer – 5'-AGAGAGACGAGTTCTCCTACC-3';
reverse primer – 5'-CCCGATGATCAGCACCTTTCG-3'.
TERT: forward primer – 5'-ATCCTGGCCAAGTTCCTGCAC-3';
reverse primer – 5'-CAACTTGCTCCAGACACTCTTC-3'.
ACTB (Calderon et al., 2012): forward primer – 5'-CACCATTGGCAATGAGCGGTTC-3';
reverse primer – 5'-AGGTCTTTGCGGATGTCCACGT-3'.

Ubiquitination Assay

15 million P493-6 cells were resuspended in 15 mL media and plated in 20 cm dishes. Cells were treated with 0.4% (v/v) DMSO, 10 μM **KI-MS2-008**, 10 μM MG132, or 10 μM **KI-MS2-008** and 10 μM MG132 for 4 hr. Cells were lysed in 100 μL modified RIPA buffer (200 mM NaCl, 50 mM Tris, 1% (w/v) NP-40, 0.1 g/100 mL sodium deoxycholate, protease inhibitor cocktail, phosphatase inhibitor, 0.4 μL benzonase/10 mL buffer) and lysate corresponding to 0.5 mg of total protein with 5 μL c-Myc antibody (N-262, Santa Cruz Biotechnology) or 2.5 μL normal rabbit IgG (sc-2027, Santa Cruz Biotechnology) was incubated overnight at 4°C. 25 μL Dynabeads (10007D, invitrogen) were added to antibody-protein mixture and incubated for 1 hr at 4°C. Beads were washed four times and samples were boiled in 2x SDS loading buffer (#1610737, Bio-Rad) at 90°C for 5 min. c-Myc (9E10, Santa Cruz Biotechnology) and ubiquitin (BML-PW8810-0100, Enzo) were visualized via immunoblotting.

Protein Binding Assay

Experiments were conducted at Cerep. Protein binding assay that simulates human plasma was spiked with 10 μM of compound at 1% (v/v) DMSO. A dialysate compartment was loaded with PBS. After incubation for 4 hr at 37°C, samples were taken from each compartment, centrifuged and supernatants were submitted to HPLC-MS/MS analysis.

Solubility of KI-MS2-001 in Aqueous Buffers

Compounds were prepared at 200 μM from 10 mM stock solutions. They were mixed with PBS buffer, simulated intestinal fluid (pH 6.5), or simulated gastric fluid (pH 1.2) with a final DMSO concentration at 2%. They were then incubated for 24 hr followed by HPLC analysis.

Bidirectional Permeability of KI-MS2-001

Experiments were conducted at Cerep. **KI-MS2-001** was prepared at 10 μM in HBSS-MES buffer, pH 6.5 and added to the apical side. HBSS-HEPES buffer, pH 7.4 was added to the basolateral side. Incubation was for 60 min total. Samples were taken at time zero from the donor side and at the end of the incubation from both the donor and the receiver sides. Samples were analyzed by HPLC-MS/MS.

Liver Microsome Stability of KI-MS2-001

Experiments were conducted at Cerep. **KI-MS2-001** was pre-incubated with pooled liver microsomes in phosphate buffer for 5 min at 37°C. The reaction was initiated by adding NADPH system and incubated for 0, 15, 30, 45 and 60 min. Concentration was measured by HPLC-MS/MS analysis.

Chromatin Immunoprecipitation Sequencing

ChIP-seq for c-Myc, Max, and H3K27ac was performed as in (Lin et al., 2012) with minor changes. P493-6 cells were grown to a density of 1×10^6 cells / mL prior to the start of time course. At each time point, pellets of 50 million cells were isolated and cross-linked with 1% formaldehyde (10 min) followed by quenching (125 mM glycine). Cells were washed in cold PBS and harvested by cell scraper in cold PBS with protease inhibitors (Roche). Cells were centrifuged at 1,650g for 5 min and flash frozen and stored at –80°C at 5×10^6 cells per pellet. Pellets were resuspended in cytosolic and then nuclear lysis buffer, and DNA was sheared at 4°C using a water-bath sonicator (Bioruptor, Diagenode) for 25 min at high output (30 s on, 30 s off) in 1 ml of sonication buffer supplemented with 0.5% SDS. Sonicated lysates were cleared by centrifuging at 20,000g for 10 min and incubated overnight end over end at 4°C with magnetic beads prebound with antibody. Beads were washed three times with sonication buffer, one time with sonication buffer with 500 mM NaCl added, once with LiCl wash buffer (20 mM Tris pH 8.0, 1 mM EDTA, 250 mM LiCl, 0.5% NP-40, 0.5%

sodium deoxycholate), and once with TE. DNA was eluted in elution buffer (50 mM Tris-HCl pH 8, 10 mM EDTA, and 1% SDS). Cross-links were reversed overnight at 65°C. RNA and protein were digested with 0.2 mg/ml RNase A for 2 h followed by 0.2 mg/ml proteinase K for 1 hour. DNA was purified with phenol chloroform extraction and ethanol precipitation.

The following antibodies were used: Max (sc-197 Max (C-17) lot C3016, Santa Cruz), Myc (ab56, Abcam), H3K27ac (ab4729, Abcam). Libraries for sequencing were prepared using the Rubicon Thruplex DNA-seq/FD library preparation kit. An input of 50 ng of DNA or less was used, and following ligation, libraries were amplified per the manufacturer's instructions. Amplified libraries were then size selected using AMPure beads (Agencourt AMPure XP) according to the manufacturer's instructions. Further size selection was performed using a 2% gel cassette in the Pippin Prep (SAGE Sciences) set to capture fragments of 200–700 bp in size. Libraries were multiplexed at equimolar ratios and run on a NextSeq 500 instrument (75-bp, single-end reads).

Reads were aligned to the HG19 NCBI Refseq (GRCh37) reference using bowtie2 with default parameters. Enriched regions were determined using MACS1.4.2 (Zhang et al., 2008) using a p-value threshold of 1e-9. To quantify ChIP-seq signal, we utilized the bamliquidator tool (https://github.com/BradnerLab/pipeline/wiki/bamliquidator) which reports ChIP-seq signal in units of reads per million per basepair (rpm/bp). To generate heatmaps of c-Myc, Max, and H3K27ac occupancy at active gene promoters, we first defined active genes as those with a H3K27ac enriched region in at least one sample at in the TSS +/- 1kb region (n=14,792 genes). ChIP-seq signal in units of rpm/bp was calculated in 200 bins evenly distributed across the +/-5kb region flanking the TSS. Meta representations are plotted below heatmaps and show the mean ChIP-seq signal in units of rpm/bp.

Myc-Addicted Tumor Cell Lines in Mice

Myc-addicted cell lines were derived from either *Em-tTA/tet-O-MYC* (T-ALL) or *LAP-tTA/tet-O-MYC* (HCC) mice and labeled with firefly luciferase. The minimal number of mice in each group was calculated using the 'pwr.t.test' function in the R/pwr package (R Development Core Team 2009; http://www.r-project.org; Champely, 2018). 2 x 10^6 luciferase-labeled T-ALL or HCC cells were injected intravenously (T-ALL) or subcutaneously (HCC) into 4-6 week-old male NOD-SCIDIL-2R$\gamma^{-/-}$ (NSG) mice. Engraftment and tumor progression were visualized and quantified by bioluminescence imaging (BLI) using an *in vivo* bioluminescence/optical imaging system (Ami HT, Spectral Instruments Imaging). The luminescence signal was assessed 10 min after intraperitoneal injection of 3 mg D-Luciferin (Promega) dissolved in PBS. Imaging was performed under general anesthesia with 2% isoflurane. Image analysis was performed using AmiView software (V1.7.06, Spectral Instruments Imaging). Upon detection of tumor cell proliferation by BLI (day 4), mice were injected with **KI-MS2-008**: T-ALL bearing mice received daily intravenous injections of 100 μL of either vehicle (saline) or 20 mM **KI-MS2-008**/saline; HCC bearing mice were injected intraperitoneally (5 days on, 2 days off) with 200 μL of either vehicle (10%(2-Hydroxypropyl)-β-cyclodextrin (HPBCD)/saline) or 40 mM **KI-MS2-008**/10%HPBCD/saline. Mice were imaged at the times indicated. Mouse experiments were approved by the Administrative Panel on Laboratory Animal Care (APLAC) at Stanford University, and were carried out in accordance with institutional and national guidelines.

Immunofluorescence Staining and Imaging

A conditional Myc-addicted osteosarcoma cell line was cultured on glass slides and treated for two days with either vehicle (DMSO or PBS), doxycycline (20 ng/ml), or **KI-MS2-001** analogues (10 μM). Cells were labeled with antibodies specific for α-tubulin (Anti-α-tubulin antibody, 1:1000, clone DM1A, Sigma-Aldrich, T9026) and Apex1 (Apex1 antibody, 1:200, Cell Signaling Technology, #4128). Goat anti-rabbit Alexa Fluor-546 and goat anti-mouse Alexa Fluor-647 (both from Invitrogen) were used as secondary antibodies. DNA was counterstained using Hoechst33342 (Invitrogen). Image acquisition was performed using a DMI6000B epifluorescence microscope (Leica) equipped with an HC PL APO 40x/0.85 DRY objective. Image processing was performed using ImageJ (Schneider et al., 2012).

Metabolic Stability Studies

Microsomes (pooled male and female) were prepared at Cyprotex or were purchased from a reputable commercial supplier. Microsomes (final protein concentration 0.5 mg/mL), 0.1 M phosphate buffer pH 7.4 and test compound (final substrate concentration 3 μM; final DMSO concentration 0.25 %) were pre-incubated at 37°C prior to the addition of NADPH (final concentration 1 mM) to initiate the reaction. The final incubation volume was 50 μL. A control incubation was included for each compound tested where 0.1 M phosphate buffer pH 7.4 is added instead of NADPH (minus NADPH). Two control compounds are included with each species. Each compound was incubated for 0, 5, 15, 30 and 45 min. The control (minus NADPH) was incubated for 45 min only. The reactions were stopped by transferring 20 μL of incubate to 60 μL methanol at the appropriate time points. The termination plates were centrifuged at 2,500 rpm for 20 min at 4°C to precipitate the protein. The samples were centrifuged (2,500 rpm at 4°C for 30 min) and the supernatants at each time point pooled for analysis by LC-MS/MS using Cyprotex generic methods. Following the microsomal stability assays, the time point at the 45 min sample was chosen and utilized for metabolite profiling. The 45 min sample was compared against the 0 min control sample to establish which and how many metabolites were formed. The metabolites found have been displayed as extracted ion chromatograms (XIC) and the representative mass spectra. The areas and percentages reported for the parent and metabolites have been calculated using the XIC data; it has been assumed that each metabolite has the same ionization efficiency and that the sensitivity of the metabolite has not been affected by the biotransformation. Any potential matrix effects have also been assumed to be consistent with the parent molecule. Metabolites observed at greater than 1% of the total of drug related material are reported. The parent compound and its associated metabolites produced both protonated and sodiated molecular ions with the sodium adducts being at a higher intensity; for the tabulated information the areas and associated

PPM errors have been reported from the sodium adducts. The m/z found for each metabolite in each species and its associated ppm error, have been displayed for each species from the time point showing the largest peak area. For accuracy a ppm error of less than 5 is desirable; when the response for a metabolite observed is low the ppm error maybe greater than 5. Where a metabolite has been referred to as a potential oxidation, it can refer to a potential hydroxylation, epoxidation or oxide formation. Representative collision induced dissociation (CID) mass spectra were obtained for the metabolites found. For elucidation the CID mass spectra for the protonated species provided more informative fragment ions for interpretation purposes; therefore these spectra are used.

Pharmacokinetics

KI-MS2-008 was administered orally at 0.731 mg/kg in 20% cyclodextrin + 1.4% DMSO into healthy 6-9 month-old male LSL-Kras G12D/+ ; Trp53 flox/flox mice. Blood samples were collected from animals (n=3/group) for vehicle control, 30 min, 1, 2, 4, 6 and 24 hr post-compound administration in EDTA containing tubes (VWR). Plasma was isolated from the blood samples and frozen. Subsequent LC/MS analysis was used to determine compound levels. Mouse experiments were approved by the Institutional Animal Care and Use Committee (IUCAC) at the Massachusetts Institute of Technology, and were carried out in accordance with institutional and national guidelines.

Repeat Dose Toxicity Studies

Healthy 6-9 month-old male LSL-Kras G12D/+ ; Trp53 flox/flox mice. (n=5 per group) were orally dosed with vehicle, 0.364 mg/kg or 0.731 mg/kg **KI-MS2-008** in 20% cyclodextrin + 1.4% DMSO daily for 7 days. Animal weights were acquired each day. On day 8, blood samples were collected to look at plasma concentration of compound, mice were sacrificed by CO_2 asphyxiation, liver and kidney were harvested and fixed in formalin. 24 hr later, fixed samples were transferred to 70% EtOH, embedded in paraffin, sectioned to 4 μm thick sections, stained with hematoxylin and eosin (H&E) and analyzed for microscopic signs of organ damage. Mouse experiments were approved by the Institutional Animal Care and Use Committee (IUCAC) at the Massachusetts Institute of Technology, and were carried out in accordance with institutional and national guidelines.

LC/MS Analysis of Plasma Samples

Plasma Extraction

Samples of 10 μL plasma were extracted in eppendorf tubes by quickly adding 500 μL of cold MeOH, followed by 300 μL cold water, and 500 μL cold chloroform. Tubes were vortexed at 4°C, centrifuged for 5 min at max speed at 4°C, the chloroform layer was transferred to a new tube and evaporated in a SpeedVac. Tubes were frozen at −80°C until ready for LCMS analysis.

LC/MS Conditions

Frozen samples were brought to room temperature then reconstituted in 20 μL methanol and 80 μL water. Samples were aliquoted into LCMS tubes with preslit caps and were run on C18 column with 5% acetonitrile (ACN, Sigma) in water + 0.1% formic acid (FA, Sigma) as mobile phase A and 95% ACN in water + 0.1% as mobile phase B. A linear gradient was used: 0-0.5 min 0% B; 0.5-10.5 min 0-100% B; 10.5-15.5 min 100% B; 15.5-17.5 min 100-0% B; run stopped at 23 min. Flow rate was 0.4 mL/min and injection volume was 10 μL. The mass spectrometer (Sciex API4000) was operated under multiple reaction monitoring mode scanning for the 4 most prominent fragments of the compound: m/z 105.1, 519.1, 416, 205.1. The parameters were: curtain gas 25 units; ion source gas 1, 30 units; ion source gas 2, 30 units; temperature 550°C; ion spray voltage 5500 V; declustering potential 96 V, and collision energy 57 eV.

QUANTIFICATION AND STATISTICAL ANALYSIS

For relevant experiments, number of replicates, error bars, statistical test, and *P* values are noted in the respective figure legends. Most experiments were repeated at least 3 times to establish reproducibility with the following exceptions: The RNA-seq data for Figure 5 was collected from 4 replicates treated separately, but from the same cell culture. The experiment with OS cells was performed twice. The MALDI, LC/MS, ^{15}N HMQC, and ChIP-seq data were acquired once. The flow cytometry experiment was completed once, but with 10,000 counts per data point. No data were excluded except for one data point that was determined to be an outlier and excluded from the analysis in Figure 5F. Image quantification was not blinded, but was analyzed by the same investigator in an unbiased manner. For the mouse studies, the minimal number of mice in each group was calculated using the 'pwr.t.test' function in the R/pwr package (R Development Core Team, 2009; http://www.r-project.org; Champely, 2018). Mouse images were coded with cage and mouse ID numbers, and were analyzed without knowledge of treatment group (although by the same investigator).

DATA AND SOFTWARE AVAILABILITY

R code for RNA-seq analysis is available upon reasonable request. The accession number for the RNA-seq data reported in this paper is GEO: GSE107222. The accession number for the ChIP-seq data reported in this paper is GEO: GSE125863. Full small molecule screening data sets, along with compound structures for the libraries, are available upon reasonable request.